frontiers | Frontiers in Earth Science

TYPE Original Research
PUBLISHED 13 January 2025
DOI 10.3389/feart.2024.1515685

Check for updates

OPEN ACCESS

EDITED BY
Fan Yang,
Lanzhou University, China

REVIEWED BY
Hu Li,
Sichuan University of Science and Engineering, China
Chang-Hao Xiao,
Institute of Geomechanics Chinese Academy of Geological Sciences, China

*CORRESPONDENCE
Shi Chen,
chenshi4714@163.com

RECEIVED 23 October 2024
ACCEPTED 26 December 2024
PUBLISHED 13 January 2025

CITATION
Chen S, Liang X, Song X, Zhang Y, Xie Z, Neng Y, Kang P and Zhou J (2025) A complete structural analysis of the F_I17 strike-slip fault and its hydrocarbon enrichment factors, Tarim basin, NW China.
Front. Earth Sci. 12:1515685.
doi: 10.3389/feart.2024.1515685

COPYRIGHT
© 2025 Chen, Liang, Song, Zhang, Xie, Neng, Kang and Zhou. This is an open-access article distributed under the terms of the Creative Commons Attribution License (CC BY). The use, distribution or reproduction in other forums is permitted, provided the original author(s) and the copyright owner(s) are credited and that the original publication in this journal is cited, in accordance with accepted academic practice. No use, distribution or reproduction is permitted which does not comply with these terms.

A complete structural analysis of the F_I17 strike-slip fault and its hydrocarbon enrichment factors, Tarim basin, NW China

Shi Chen[1,2]*, Xinxin Liang[1,2], Xingguo Song[1,2], Yintao Zhang[3], Zhou Xie[3], Yuan Neng[1,4], Pengfei Kang[3] and Jianxun Zhou[1,2]

[1]National Key Laboratory of Petroleum Resources and Engineering, China University of Petroleum, Beijing, China, [2]College of Geosciences, China University of Petroleum, Beijing, China, [3]PetroChina Tarim Oilfield Company, Korla, China, [4]Department of Geoscience, China University of Petroleum at Karamay, Karamay, China

The F_I17 fault is a prominent strike-slip fault in the central Tarim basin, notable for its hydrocarbon abundance and intricate tectonic attributes, characterized by several deflections in its planar trajectory. Analyzing the F_I17 fault offers crucial insights into the role of basement structures on the evolution and formation of intracratonic strike-slip fault systems. This study utilizes the latest seismic data and integrating the foundation of previous research to conduct a detailed investigation into the spatial distribution, deformation intensity, activity phases, and formation mechanisms of the fault. The fault can be divided into three structural layers based on deformation features. The deep layer, situated beneath the $T\epsilon_3$ interface (the bottom of the Upper Cambrian), shows basement rifts and weak strike-slip activity. The middle layer, spanning from $T\epsilon_3$ to TO_3 (the bottom of the Upper Ordovician), exhibits pronounced deformation with flower-like structures. The upper layer, extending from the TO_3 to TP (the bottom of the Permian), is marked by three groups of en-echelon normal faults. Controlled by Precambrian basement heterogeneity, the fault evolved through three stages: weak compressive stress during the Middle -Late Cambrian led to rupture along basement rifts and weak zones that formed the fault's embryonic shape; strong compressive stress from Middle-Late Ordovician activated and propagated the fault upwards; during the Silurian-Carboniferous, the fault experienced episodic reactivation and result in the emergence of en-echelon normal faults. Hydrocarbon enrichment at the F_I17 fault is influenced by source rock distribution, reservoir characteristics, and fault reactivation. Its positioning above the source rock center ensures an ample supply of hydrocarbon. The intense fault activity has created favorable conditions for large-scale fracture-cavity reservoir development, and the reactivation period corresponds with the hydrocarbon accumulation phase, significantly boosts hydrocarbon charging.

KEYWORDS

Tarim basin, layered deformation, basement structure, formation mechanism, hydrocarbon enrichment

1 Introduction

Oil and gas accumulation in the central Tarim basin is notably affected by the presence of strike-slip faults, along which a considerable number of highly productive wells have been developed (Deng et al., 2019; Tian et al., 2021; Wang et al., 2021). Several oilfields have been established in the vicinity of these fault, such as the Shunbei and Fuman oilfields (Qi, 2020; Wang et al., 2022; Liu et al., 2023). Evidence suggests a strong correlation between strike-slip faults and the occurrence of ultra-deep Ordovician karstic carbonate reservoirs (Jiao, 2017; Deng et al., 2018; Tian et al., 2021). The characteristics of reservoirs that are controlled by small to medium slip distance strike-slip faults in the Tarim basin have been continuously verified. The fault-controlled fracture-vuggy type reservoirs have emerged as the primary target for the exploration and development of ultra-deep carbonate hydrocarbon reserves in the Tarim basin (Wang et al., 2017; Qi, 2020; Deng et al., 2021). In recent years, the Fuman oilfield of the China National Petroleum Corporation (CNPC) has developed a number of petroliferous fault zones, including the F_I5, F_I10 and F_I17 faults, encompass more than 10,000 km^2 of reservoirs and represent the largest oil exploration discoveries in the Tarim basin over the past decade (Wang et al., 2021; Liu et al., 2023).

Previous scholars have extensively delved into the study of strike-slip faults in the central Tarim basin. Their endeavors have yielded significant advancements, including the classification of fault with development scales, the zoning of strike-slip fault systems, the layered deformation structure, the deformation phases, and the segmentation of planar features (Wu et al., 2012; 2019; 2020a; Wang B. et al., 2020; Teng et al., 2020; Sun et al., 2021; Chen J. J. et al., 2022; Neng et al., 2022; Yao et al., 2023). Moreover, new insights have been proposed into the development of faults and fractures in tight reservoirs, and enrichment processes of hydrocarbon (Li et al., 2019; Tian et al., 2021; Wang et al., 2021; Wang et al., 2022; Deng et al., 2022; Fan et al., 2024). The F_I17 fault stretches over 200 km from the Tazhong Uplift to the Manxi Low Uplift, recognized as one of the large petroliferous fault that the Fuman Oilfield has successfully exploited to date (Liu and Deng, 2022; Li et al., 2023). Along the fault, the MS1, MS3, and MS4 wells have been drilled, each yielding an impressive output of over 1,000 tons of oil and gas equivalent daily (Tian et al., 2021; Wang et al., 2022).

Predecessors have conducted a series of researches on the F_I17 fault and achieved significant insights. On the section, the fault is characterized by sub-vertical strike-slip faults and en-echelon normal faults; on the plane view, it is marked by three stress regimes labeled "transpression, transtension, and translation" (Liu and Deng, 2022; Li et al., 2023). The fault serves as a link between the strike-slip fault systems of the Tabei and Tazhong uplifts, and it is characterized by the connection of multi discrete fault segments during evolution (Liu and Deng, 2022). Nonetheless, debates persist concerning the onset of fault activity, with opinions divided between the Middle-Late Cambrian (Song et al., 2023; Wang, 2023) and the Middle-Late Ordovician (Liu and Deng, 2022; Li et al., 2023). The central Tarim basin is extensively characterized by Precambrian basement rifts (Neng et al., 2022), which have significantly impacted the development and evolution of strike-slip faults (Han et al., 2017; Song et al., 2024b). However, the influence of the basement rifts on the F_I17 fault remains unclear. Additionally, the principal factors responsible for the fault plane's intricate deflections remain obscure, and the controlling factors for the enrichment of hydrocarbon need further investigation.

In this study, we have systematically interprets the geometrical characteristics of the fault, and the fault activity pattern has been utilized to delineate the various deformation stages of the fault. Additionally, the distribution characteristics of the basement rifts has been emphasized to elucidates the fault's formation mechanism. Concurrently, the features of source rocks, the characteristics of fault development, and the phases of hydrocarbon generation have been integrated to provide a comprehensive analysis of the hydrocarbon accumulation process. We show that the F_I17 fault was active from the Middle to Late Cambrian, with its evolution and formation mechanism jointly controlled by the activity of peripheral orogenic belts and the distribution of basement rifts. Importantly, these basement rifts determined the favorable location for faults development, and the strike-slip faults exhibit characteristics of segmented linking and growth. The basement rifts underlying the F_I17 fault are distributed in a non-linear pattern, leading to multiple deflections in the fault's planar trajectory.

This research is driven by the following principal aims: 1) to develop a model illustrating the spatial differential development of faults; 2) to elucidate the various phases of fault deformation and the onset of fault activity, 3) to delineate the formation mechanism and evolution processes influenced by the Precambrian rift system; 4) to explore the key factors that govern hydrocarbon enrichment within the Fuman Oilfield.

2 Geological setting

Covering an area of approximately 400,000 km^2 in southern Xinjiang, the Tarim Basin is a notable superimposed basin in China with considerable hydrocarbon resources (Tang, 1994; Jia, 1997; Jia and Wei, 2002; He et al., 2005). The Manxi Low Uplift is located between the Tabei uplift and the Tazhong uplift, flanked by the Manjia Depression to the east and the Awati Depresssion to the west (Figure 1A). This paper focuses on the F_I17 fault, which stretches for over 200 km with an S-shaped trajectory, traversing the Tazhong Uplift and the Manxi Low Uplift. The fault serves as a pivotal link between the simple shear strike-slip system in the south and the pure shear strike-slip system in the north, essential for the transfer of strain and the accommodation of displacement (Sun et al., 2021) (Figure 1B).

The Tarim Basin's sophisticated tectonic is profoundly affected by the orogenic activities encircling it. With the disintegrate of the Rodinia supercontinent, the Tarim block rose, establishing the early crystalline basement of Archean-Neoproterozoic (Zhang et al., 2007; Wu et al., 2018). The craton was ringed by paleo-oceans, namely the South Tianshan Ocean to the north, the ancient Kunlun Ocean to the southwest, and the Altun Ocean to the southeast (Mattern and Schneider, 2000; Li et al., 2009; Zhang et al., 2009). Characterized as a passive continental margin, the basin's geotectonic background experienced a pervasive extensional stress from the Precambrian through the early Ordovician (Li et al., 2013; Gao and Fan, 2014). During the Middle to late Ordovician, the ancient Kunlun and Altun Oceans initiated subduction process under the Tarim plate (Zhang et al., 2002; Li et al., 2009), effecting a tectonic reorientation.

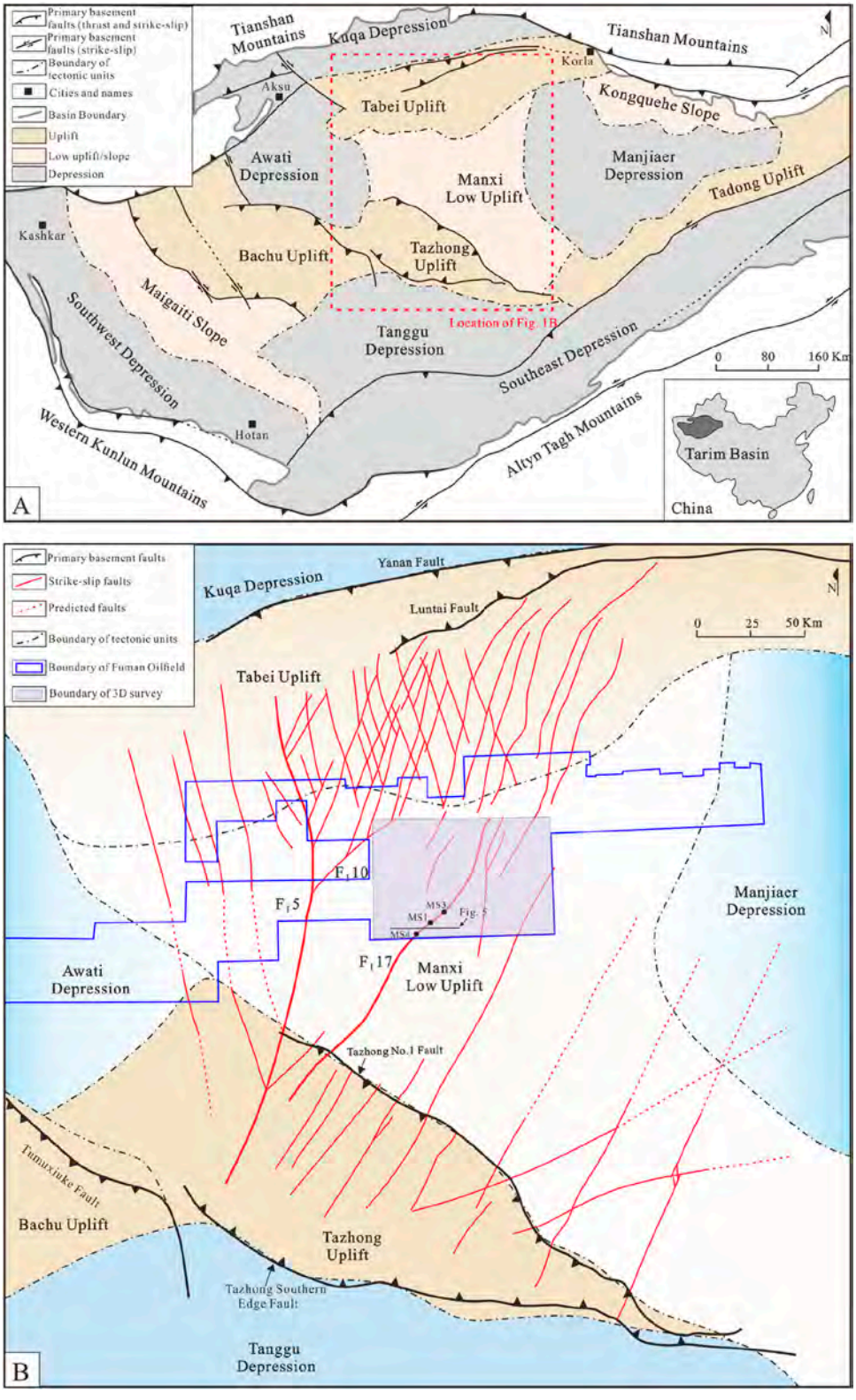

FIGURE 1
(A) Simplified distribution map of the major tectonic units in the Tarim Basin (Modified from Li et al., 2013); **(B)** tectonic map showing the major tectonic units and fault distributions in the central Tarim Basin (revised after Deng et al., 2019; Wang B. et al., 2020; Chen et al., 2024).

This led to a compressional tectonic phase during the Silurian, characterized by intense orogeny in the Altun domain (Yang et al., 2005; Liu et al., 2007), and the formation of the Tabei and Tazhong uplifts (Wang, 2004; Ren et al., 2011). The South Tianshan Ocean underwent a progressive east-to-west closure during the Silurian, culminating in its complete closure in the Carboniferous (Allen et al., 1993; Gao et al., 2006; Han et al., 2011). By the Permian, with the closure of the surrounding oceans, the Tarim Basin had evolved into an intracontinental depression (Yang et al., 2005), with widespread volcanic activity influenced by the associated large igneous province (Sharps et al., 1989; Li et al., 2011; Xu et al., 2021). In the Triassic, the basin underwent significant compression, uplift, and erosion due to tectonic movements related to the Paleo-Tethys block to the south (Yu et al., 2014). A period of weak extension characterized the Jurassic (Zhang et al., 2007; Zheng et al., 2014). During the Cenozoic, significant uplift and erosion occurred within the basin, a consequence of the far-field impacts from the collision between the Indian and Eurasian plates (Windley et al., 1990; Li et al., 2012; Zhu et al., 2022). The tectonic event has persistently influenced the geological and morphological features of the Tarim Basin, shaping it into its present form.

The Paleozoic to the Cenozoic strata was well developed in the Manxi low uplift. Within the Paleozoic strata, a gradual transition of sedimentary facies is observed. The shift progresses from carbonate platform facies at the Cambrian-Middle Ordovician to clastic littoral neritic facies at the Upper Ordovician-Carboniferou, indicative of a dynamic evolutionary process in the basin's depositional environment. The Cambrian to Middle Ordovician deposited thick carbonate rocks and the Late Ordovician developed regional thick mudstones. Silurian to Carboniferous clastic rocks were extensively developed, and Permian volcanism was frequent, with widespread deposition of igneous rocks (Figure 2). The Cambrian strata in the region are sequentially composed from the base upward of the Yuertusi Formation ($\in_1$y), the Xiaoerbulake Formation ($\in_1 x$), the Wusonggeer Formation ($\in_1 w$), the Shayilike Formation ($\in_2$s), the Awatage Formation ($\in_2$a) and the Lower Qiulitage Formation ($\in_3 q$) (Chen et al., 2024). Continuing upwards, the Ordovician sequence is stratified, starting with the Penglaiba Formation ($O_1 p$), Yingshan Formation ($O_{1\text{-}2} y$), Yijianfang Formation (O_2y), Tumuxiuke Formation ($O_3 t$), Lianglitage Formation ($O_3 l$) and Sangtamu Formation (O_3s) (Figure 3). The exploration and development efforts within the Fuman oilfield are predominantly focused on the Yijianfang Formation (O_2y) and the upper part of the Yingshan Formation ($O_{1\text{-}2}$y), which are identified as the principal target formations. The Lower Cambrian Yuertusi Formation ($\in_1$y) is recognized as the primary source rock, endowing the area with significant hydrocarbon generation potential. Additionally, the extensive development of thick mudstones within the upper Ordovician Sangtamu Formation (O_3s) provides an advantageous cap rock condition. Collectively, these strata constitute a critical source-reservoir-caprock ensemble that is vital for the hydrocarbon prospectivity of the Fuman oilfield (Tian et al., 2021).

3 Data and methodology

The research is based on 3D seismic data of Fuman oilfield provided by CNPC and loaded using Landmark software (Figure 3). The 3D survey, with a rectangle area of 50×80 km, covers the northern part of the F_I17 fault. The inlines of the survey are east-oriented and intersect with fault strike at a large angle, which act as the dominant seismic profile interpretation direction with a spacing of 100 m. Based on the acquired well logs and "well-seismic" calibration, critical seismic reflection interfaces are correlated to corresponding stratigraphic units, including the bottom of the Cambrian ($T\in_1$), the bottom of the Middle Cambrian ($T\in_2$), the bottom of the Upper Cambrian ($T\in_3$), the bottom of the Ordovician (TO), the bottom of the Upper Ordovician (TO_3), the bottom of the Silurian (TS), the bottom of the Devonian (TD), the bottom of the Carboniferous (TC), and the bottom of the Permian (TP). Seismic coherence volume was calculated with Landmark software, and slices were extracted to identify fault in the plane view, encompass the interface $T\in_3$, interface TO_3, interface TS and interface TC. On the cross section, the break of seismic reflecting surface and chaotic seismic reflection in bead-string are typical indicatives of strike-slip fault planes. To discern the spatial variations in deformational intensity, this study meticulously measures the vertical separation and fault throw associated with the key interfaces: $T\in_3$, TO_3, TS, and TC, aim to highlight the disparities in the degree of deformation across different interfaces.

These measurements have enabled a detailed analysis of the F_I17 fault's geometry and kinematics within the 3D survey, allowing us to pinpoint the active phases of its evolution history. Additionally, by correlating with Precambrian rifts distribution patterns, the formation mechanism can be proposed from a new insight. Combined with the distribution pattern of source rock, the characteristics of fracture development and the features of corresponding hydrocarbon reservoirs, to discuss the key factors that govern hydrocarbon enrichment within the Fuman Oilfield.

4 Fault geometry characterization of F_I17 strike-slip faults

4.1 Geometry of the F_I17 strike-slip faults in plane view

Spanning over 200 km in plan view, the F_I17 fault traverses the Manxi Low Uplift, situated between the Tazhong Uplift and the Tabei Uplift (Figure 1B). Within the 3D survey of the Fuman Oilfield, the fault stretches approximately 70 km, exhibiting multiple directional changes along its strike. The southern segment of the fault aligns in NE direction, while the northern segment progressively shifts counterclockwise towards a N-S orientation, marked by a striking variation from NE50° to NE33° and finally to NE8° (Figure 4A). Considering the distinct strike variation characteristics, the F_I17 fault in Fuman Oilfield can be delineated into three distinct parts: the northern, middle, and southern.

The feature of F_I17 strike-slip varies across distinct interfaces. In order to better distinguish the fault patterns in varied depth, four interfaces, the bottom of Upper Cambrian ($T\in_3$), the bottom of the Upper Ordovician (TO_3), the bottom of Silurian (TS) and the Carboniferous basement (TC), were selected in this study to present fault features in comparison, based on detailed seismic interpretation (Figure 4).

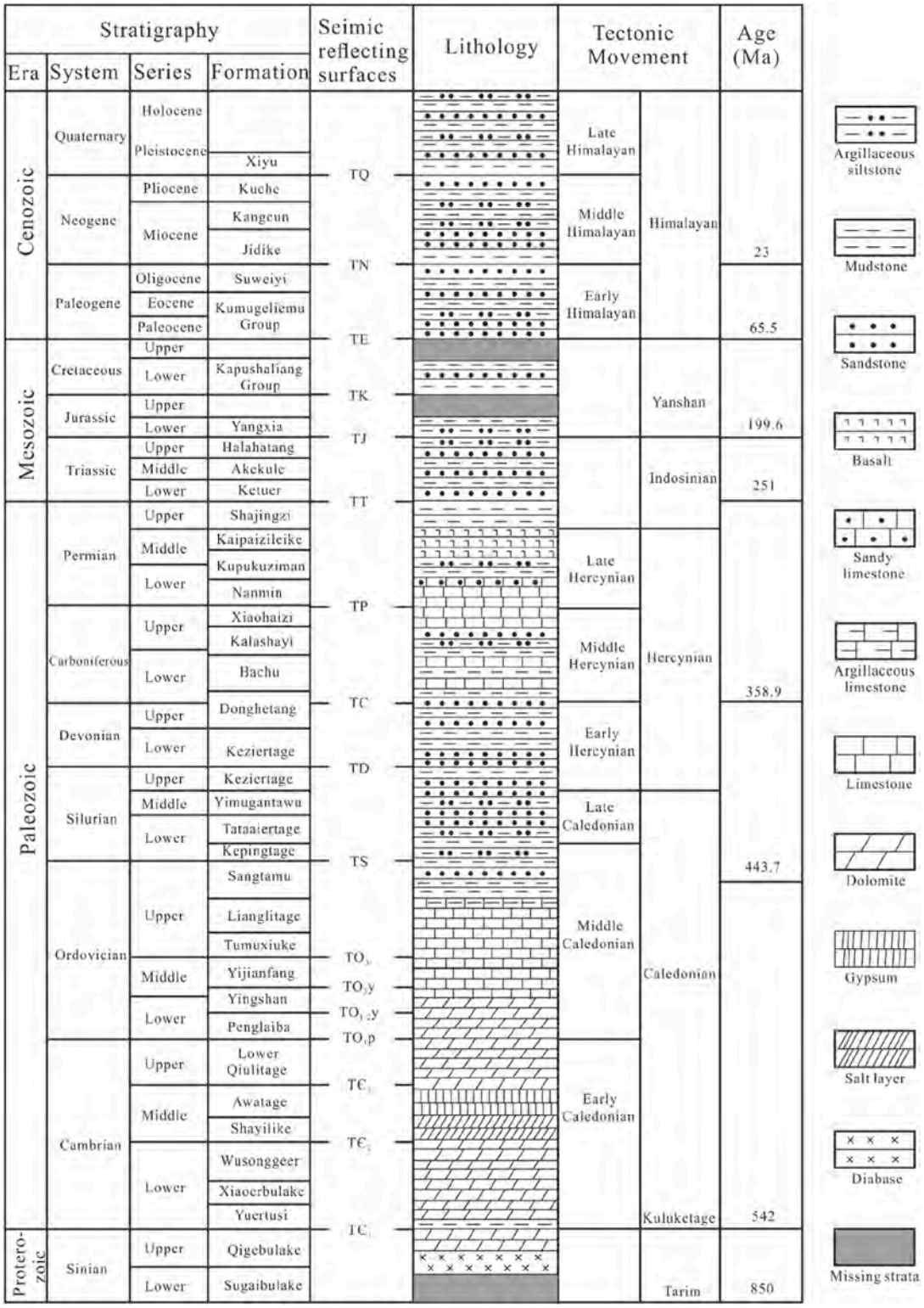

FIGURE 2
Simplified stratigraphic framework of Fuman oilfield and its adjacent area (Modified after Deng et al., 2019; Neng et al., 2022).

On the Tϵ_3 interface (Figures 4B, B'), the F_I17 fault extends linearly, composed of distinct segments linked by soft connections. In the southern part, left- and right-stepping are developed alternately in the overlapping zone, whereas the northern and middle parts exhibit a predominantly left-stepping arrangement. At the junction between the southern and middle parts, left-stepping

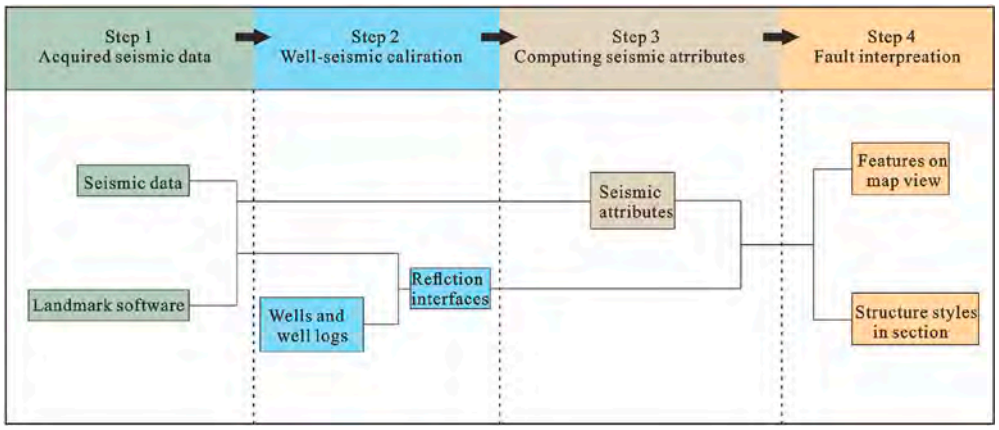

FIGURE 3
Simplified seismic interpretation flowchart for strike-slip fault in the central Tarim basin (Modified after Song et al., 2024a).

en echelon faults is oriented in the NW direction. Prolonged linear branch faults are also observed flanking both sides of the middle and northern parts. The coherent slice characteristics reveal a significant anomaly in the strike-slip deformation zone within the southern part, which diminishes progressively through the middle to the northern part and the deformation width also correspondingly narrows.

On the TO_3 interface (Figures 4C, C'), compared to the $T\epsilon_3$ interface, there is an enhancement in fault activity, with segments interconnected through both soft and hard linkages. Along the southern part, the structural patterns transition from rhomboidal to braided structures from south to north, which are continuously developed on the planar surface and are distributed in a "candied hawthorn" pattern, correlating with topographic features (Figures 4A, A'). The middle and northern parts primarily exhibit linear shape structure, wherein the middle part's overlap zone alternates between left- and right-stepping, while the northern part are predominantly arranged in a left-stepping sequence. Linear branch faults persistently evolve, particularly around the junction of the middle and northern parts. Volcano-related dome structures, measuring approximately 1 km in diameter on the plan view, are widely disseminated, with a high concentration along the peripheries of the northern and middle parts of the fault.

At the TS (Figures 4D, D') and TC (Figures 4E, E') interfaces, the faults display a consistent development pattern. The echelon normal faults are neatly aligned in a sequential order, the length of each echelon fault expands from the south to the north, with an average increase from 3 km to 10 km. The density of these echelon faults gradually diminishes northward, with an increase in the spacing between them. The echelon fault development in the northern part does not perfectly align with the underlying vertical strike-slip fault. Instead, it is predominantly situated between the F_I17 and the adjacent F_I19 fault, attributed to the mutual influence and activation of these two faults, suggesting a sophisticated interplay in their formation and evolution.

4.2 Structural styles of F_I17 fault in seismic sections

The strike-slip faults within the central Tarim Basin are characterized by a distinct pattern of layered deformation (Han et al., 2017; Deng et al., 2019). Classifying these faults based on their deformation style, variations in lithology, and evolutionary timeframes, researchers have categorized the strike-slip faults into configurations of two (Han et al., 2017; Deng et al., 2019; Sun et al., 2021), three (Chen et al., 2024; Song et al., 2024a), and four distinct layers (Neng et al., 2022; Shen et al., 2022). In the seismic profiles, the F_I17 fault is observed to exhibit flower structures, with echelon normal faults clearly extending from the Upper Ordovician to the Carboniferous (Figure 5A). These structures present a multi-layered architecture and display varied deformation patterns across different strata. Utilizing the distinct structural styles and key lithological boundaries, namely the $T\epsilon_3$ and TO_3 interfaces, the F_I17 fault's layered deformation model can be delineated into deep, middle, and upper structural layers (Figure 5B).

The deep structural layer consists of the Precambrian basement, Lower-Middle Cambrian strata (below $T\epsilon_3$). Rifts and paleo-uplifts are widely distributed in the Precambrian basement, and the strike-slip faults generally present a subvertical fault plane. The plastic deformation of the gypsum-salt layer is complicated by the action of strike-slip faults, with local thickening, thinning, development of salt arches and small reverse faults. The middle structural layer consists of Upper Cambrian-Middle Ordovician carbonates ($T\epsilon_3$-TO_3). The main faults and branching faults form flower structure, and the strike-slip faults generally end near the TO_3, and the lower part of Upper Ordovician mudstones was also deformed by the faults. The upper structural layer is composed of clastic rocks ranging from the Upper Ordovician to the Carboniferous (TO_3-TP). Echelon normal faults, a result of reactivated strike-slip faults, are extensively developed, giving rise to graben and half-graben structures. Some of these faults extend deep, penetrating the TO_3 interface and intersecting with the positive flower structure beneath, give rise to the formation of composite flower structure.

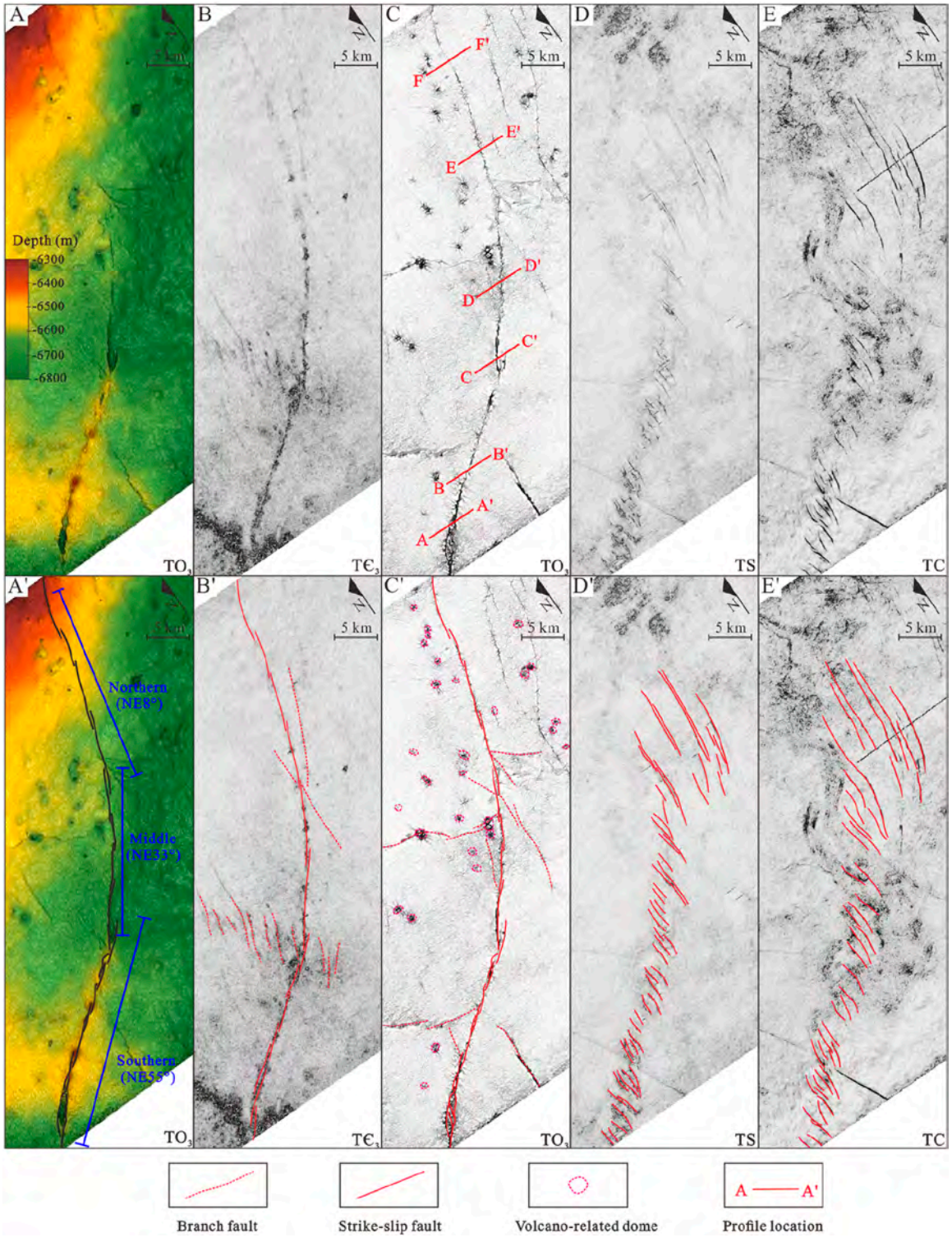

FIGURE 4
Spatial distribution of the F_I17 strike-slip fault in Fuman Oilfield. Uninterpretated structural map **(A)** of seismic interface TO3 and associataed fault interpreatation **(A′)**; Uninterpreted coherence slices of seismic interface TЄ3 **(B)**, TO3 **(C)**, TS **(D)**, TC **(E)** and associated fault interpretation **(B′–E′)**.

At the southern part of the F_I17 fault, intense fault activities have taken place in both the deep and upper layers, characterized by significant deformation amplitudes (Figures 6A, B). In the deep structural layer, the strike-slip faults penetrate directly into the basement, situated at the edge of a paleo-uplift or along slope. Near the $T\epsilon_3$ interface, secondary faults are prevalent,

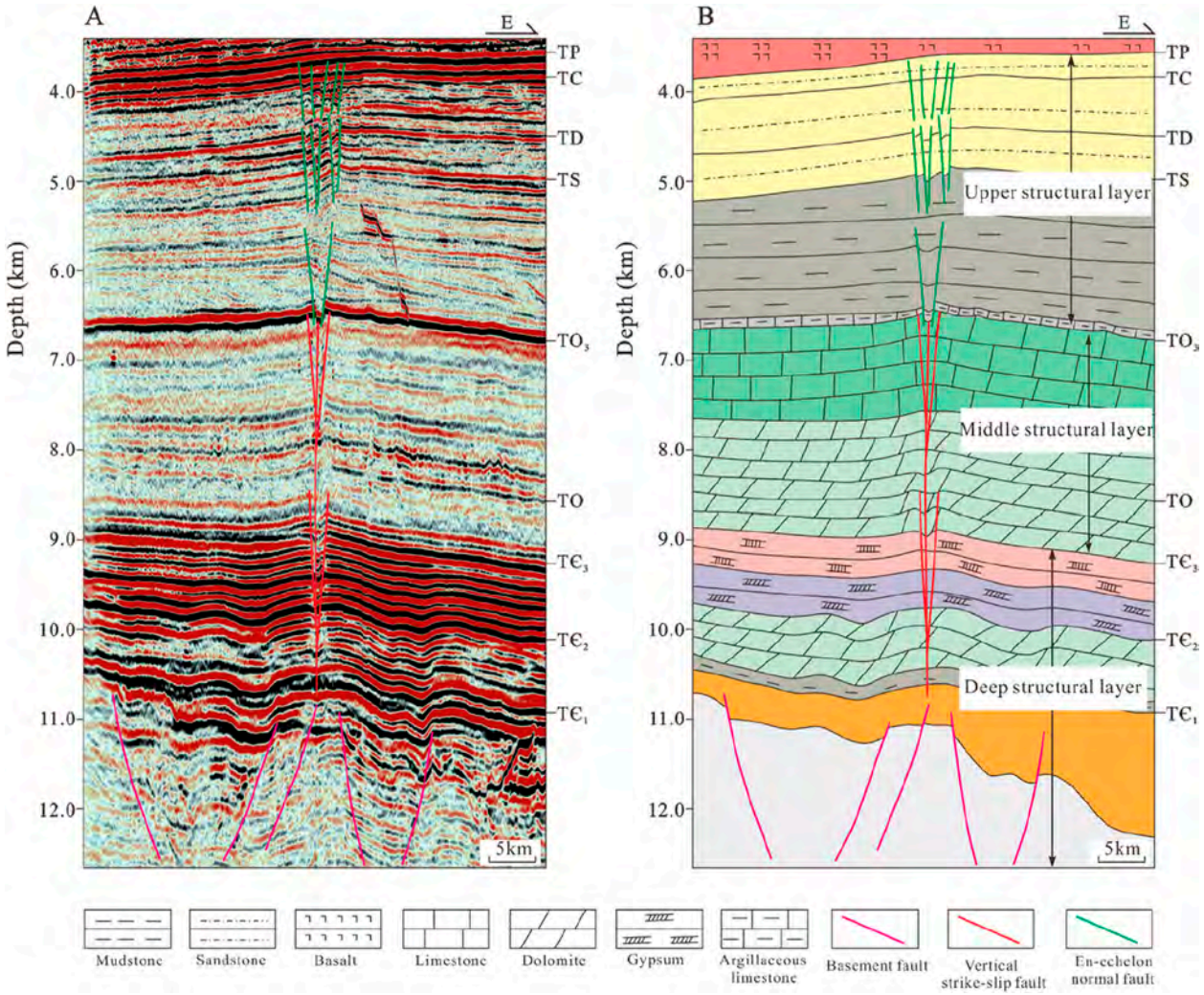

FIGURE 5
Typical seismic profile **(A)** of F_I17 strike-slip fault in Fuman Oilfield and layered deformation model **(B)**. (for location, see Figure 1B).

converging to form flower structure, predominantly manifesting as negative structures, with salt sag emerged in the Middle Cambrian gypsum-salt layer within the deformation zone (Figure 6A). In the middle structural layer, the strike-slip faults exhibit clear fault displacements, beaded reflection and chaotic seismic reflections on the seismic profile. There is intense deformation near at the TO_3 interface, accompanied by branch faults and flower structures, and the stress environment shift from transtension to tranpression from south to north. Close to the TO interface, branch faults are also evident, converging to form a complex multi-layered flower structure. In the upper structural layer, three groups of normal faults are distinguished based on their cut-through horizons and distribution sequence. The lower group of normal faults is developed above the segments in strong tanstension environment and is distributed within the Upper Ordovician, cutting through the TO_3 interface and forming a composite flower structure. The middle and upper groups of normal faults are developed more densely, and the middle group extends downward into the Upper Ordovician and terminates upward in the Devonian, while the upper group is primarily located within the Devonian-Carboniferous.

In the middle part of the F_I17 fault (Figures 6C, D), the lower structural layer exhibits share similar characteristics with the southern part. The strike-slip faults penetrate vertically into the basement, positioned along the slope. Adjacent to the $T\text{Є}_3$ interface, branch faults are developed, predominantly under weak transpression environment, giving rise to positive flower-structures and the formation of salt dome structures. In the middle structural layer, there is a discernible northward stress environment shift from strong transtension to weak transpression, and a substantial negative flower structure (Figure 6C), display pronounced downward deformation, transitioning northward into positive flower structures (Figure 6D), with the upper arch of these strata experiencing minimal deformation. In the upper structural layer, reflecting the pattern observed in the southern part, the normal faults can be categorized into three distinct groups. The lower group is situated within the Upper Ordovician, above a segment of intense transtension, where inverse drag fold

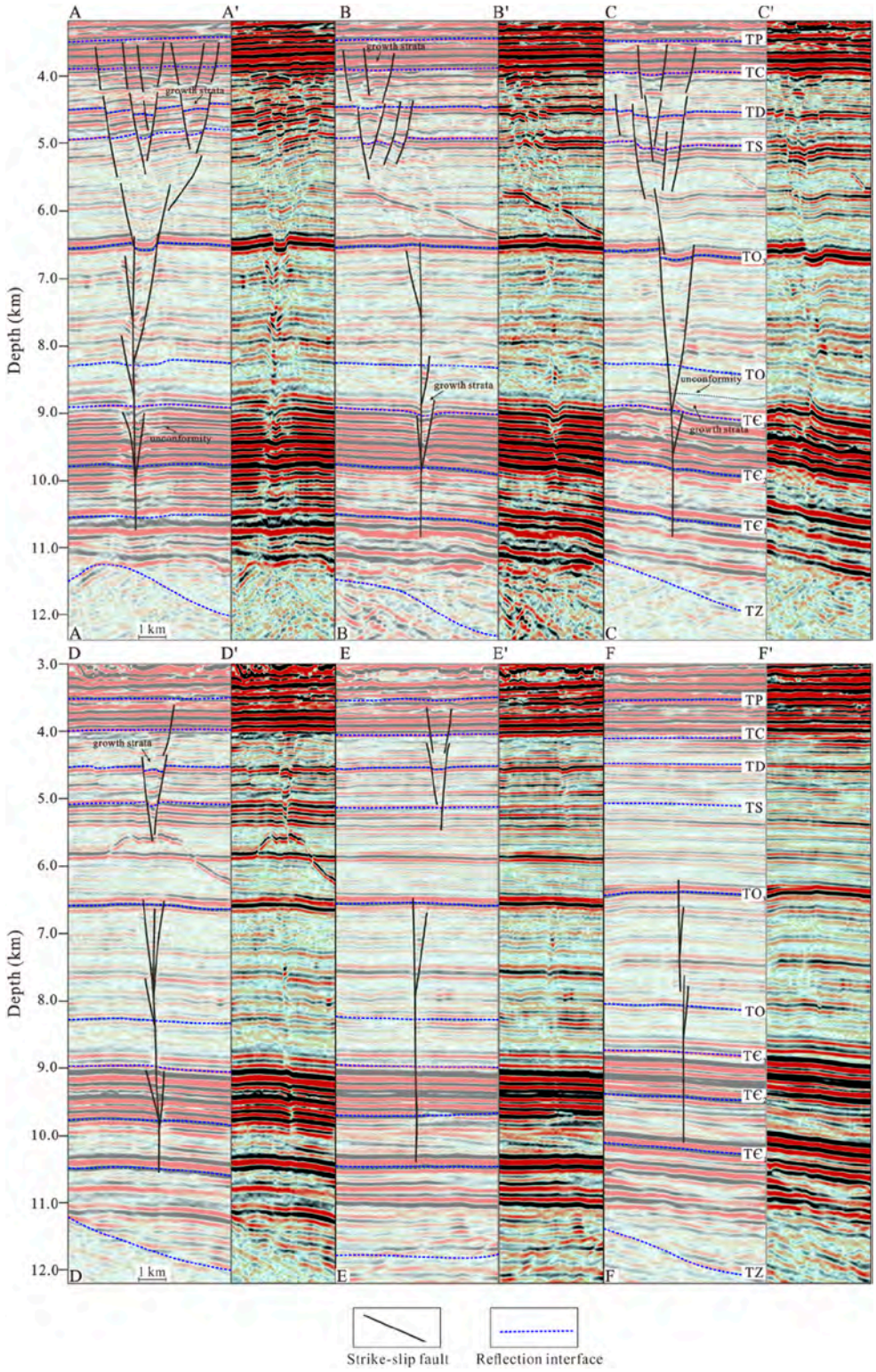

FIGURE 6
3D seismic profiles and corresponding fault interpretations of $F_1$17 fault in the Fuman Oilfield **(A–F)**. (Cross sections are W-E oriented and transect the main PDZ, see Figure 4 for section locations).

and synsedimentary thickening strata are prominently developed. Moving from south to north, there is a gradual decrease in fault density and fault displacement within the middle and upper group.

In the northern part of the $F_1$17 fault (Figures 6E, F), within the lower structural layer, the strike-slip fault rests on the basement slope and flat sediment area, and the subtle curvature of the seismic

phase axis indicate the fault plane, without branching faults present. In the middle structural layer, the faults predominantly manifest as upright strike-slip, with branch faults that interconnect to create a semi-flower structure, and there is a progressive attenuation of fault activity northward, showcasing features indicative of vertical superimposed growth (Figure 6F). In the upper structural layer, the normal faults are partitioned into two groups, confined to the Upper Ordovician-Devonian and Devonian-Carboniferous, with subdued activity and sparse distribution (Figure 6F), and these faults are gradually vanishing northward.

5 Deformational magnitude of the F_I17 fault

The fault activity intensity of the F_I17 fault (Shunbei No. 4 fault) has been thoroughly investigated by previous researchers from various perspectives, including the vertical separation amplitude, width of deformation zone, and fault throw (Liu and Deng, 2022; Li et al., 2023; Liu et al., 2023). Building upon this foundational work, the study investigation quantifies the deformation magnitude along the F_I17 fault within the Fuman Oilfield and the Tazhong Uplift in critical interfaces. By integrating previous findings, especially the F_I17 fault activity intensity pattern in Shunbei Oilfield (Liu and Deng, 2022; Li et al., 2023), a comparative analysis is conducted, to reveal the variance of the fault activity intensity along the strike in $T\epsilon_3$, TO_3 and TS interfaces (Figure 7).

At the bottom of the Upper Cambrian ($T\epsilon_3$ interface), the F_I17 fault exhibits a consistent and modest vertical separation amplitude along the strike, and diminishes gradually northward in Fuman Oilfield. The positive and negative deformation are interspersed, with the absolute value predominantly within the range of 100 m (Figure 7A). Notably, the deformation amplitude reaches its zenith at the segment of the fault plane that experiences strike deflection, where it can locally peak at 200 m. The pronounced peak is associated with the stress concentration and release that occur as a result of the strike deflection of the strike-slip fault.

At the bottom of the Upper Ordovician (TO_3 interface), F_I17 fault displays a consistent vertical separation amplitude along the strike within the Tazhong uplift, mirroring the conditions observed at the bottom of the Upper Cambrian ($T\epsilon_3$ interface), with the absolute values confined within a 100 m. Nonetheless, as the fault trace crosses the TZ1 fault and proceeds into the Manxi Low Uplift, there is a marked escalation. Pronounced peaks occurred at the inflection point of fault plane, with deformation amplitudes soar to 200–300 m, and the values gradually taper off as further north into the Fuman Oilfield (Figure 7B).

At the bottom of the Silurian (TS interface), within the Tazhong Uplift, the overall characteristics of fault throw are consistent with those at the bottom of the Upper Cambrian ($T\epsilon_3$ interface), exhibiting a small and uniform fault throw with an average of approximately 20 m. Upon crossing the TZ1 fault and entering the Manxi Low Uplift, the fault throw increases significantly and shows vertical inheritance with the TO_3 interface, particularly where there is a change in the fault's strike, the fault throw reaches its peak values of 60–80 m (Figure 7C), and it gradually decreases from south to north within the Fuman Oilfield.

6 Active stages of F_I17 fault

Extensive research has been dedicated to research on the active stages of strike-slip faults in the central Tarim basin, with the consensus that the earliest period of fault activity dated back to the Middle (Sun et al., 2021; Yao et al., 2023) or Late Ordovician (Han et al., 2017; Deng et al., 2019; Shen et al., 2022). However, recent studies have revealed the presence of a localized compressive stress environment within the basin during the Cambrian (Xu et al., 2011; Ge et al., 2014; Chen et al., 2024), which suggests that the initial activity of the strike-slip faults may be traced back to the Cambrian (Teng et al., 2020; Chen et al., 2024; Song et al., 2024a). This study based on the development characteristics of the fault, growth strata and unconformity features, deformation phases of the F_I17 fault in the Fuman Oilfield can be categorized into three stages: Middle to Late Cambrian, Middle to Late Ordovician, and Silurian to Carboniferous (Figure 8).

The embryonic stage of the F_I17 fault occurred during the Middle to Late Cambrian (Figure 8A). During the period, the fault exhibited relatively low activity, and deformation was primarily concentrated near the bottom of the Upper Cambrian ($T\epsilon_3$ interface), with localized development of branch faults that interconnected to form a flower-structure. There were also characteristics indicative of reverse superposition of flower-structure features, such as the positive deformation in the Ordovician and negative deformation in the Cambrian (Figure 6B) and the negative deformation in the Ordovician and positive deformation in the Cambrian (Figure 6C), which suggest that the stress environment during the Middle-Late Cambrian was distinct from later periods. As a result of the fault activity during the Middle-Late Cambrian, which led to the formation of flower-structures, the strata experienced positive or negative deformation, give rise to the development of growth strata within the negative flower-structure's deformation zone (Figure 6B), and the development of an unconformity between the top of the positive flower-structure and the overlying strata (Figure 6C).

The mature stage of F_I17 fault activity is Middle to Late Ordovician (Figure 8B). During the period, the fault activity was robust, with flower-structures were generally formed near the bottom of the Upper Ordovician (TO_3 interface), resulting in the positive deformation of the TO_3 interface and the adjacent overlying strata, or negative deformation of the TO_3 interface and the development of normal faults within the Upper Ordovician, leading to the formation of grabens and half-grabens (Figures 6A, C). The TO_3 interface shows the greatest deformation amplitude, indicating that the fault was most active at the end of the Middle Ordovician and continued its activity into the Late Ordovician.

The reactivation stage of the F_I17 fault spans from Silurian to Carboniferous (Figure 8C). In the upper structural layer, the middle and upper groups of normal faults are associated with the reactivation of vertical strike-slip faults. Along the profile, there is evidence of growth strata within the grabens and half-grabens, shaped by the interplay of normal faults. The presence of growth strata in the Silurian, Devonian, and Carboniferous (Figures 6A, B) suggests that the active period for these groups of normal faults extends continuously from the Silurian through to the Carboniferous. The vertical layered discontinuity of the two groups

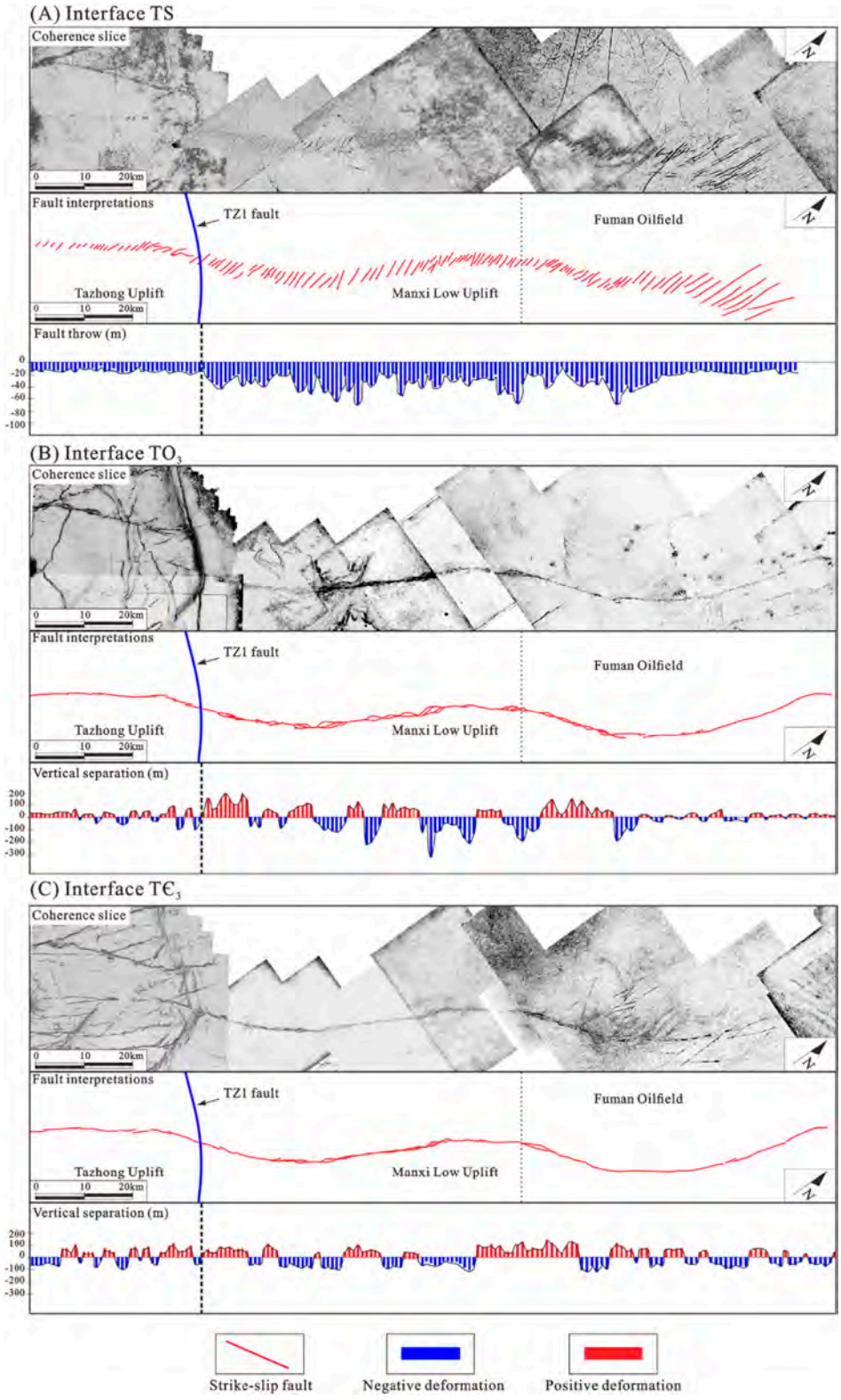

FIGURE 7
Fault throw at interface TS **(A)**, and vertical separation at interfaces TO_3 **(B)** and $T\epsilon_3$ **(C)**, showing the variation in deformation magnitude along strike the $F_1$17 fault at critical interfaces (Modified from Liu and Deng, 2022; Li et al., 2023).

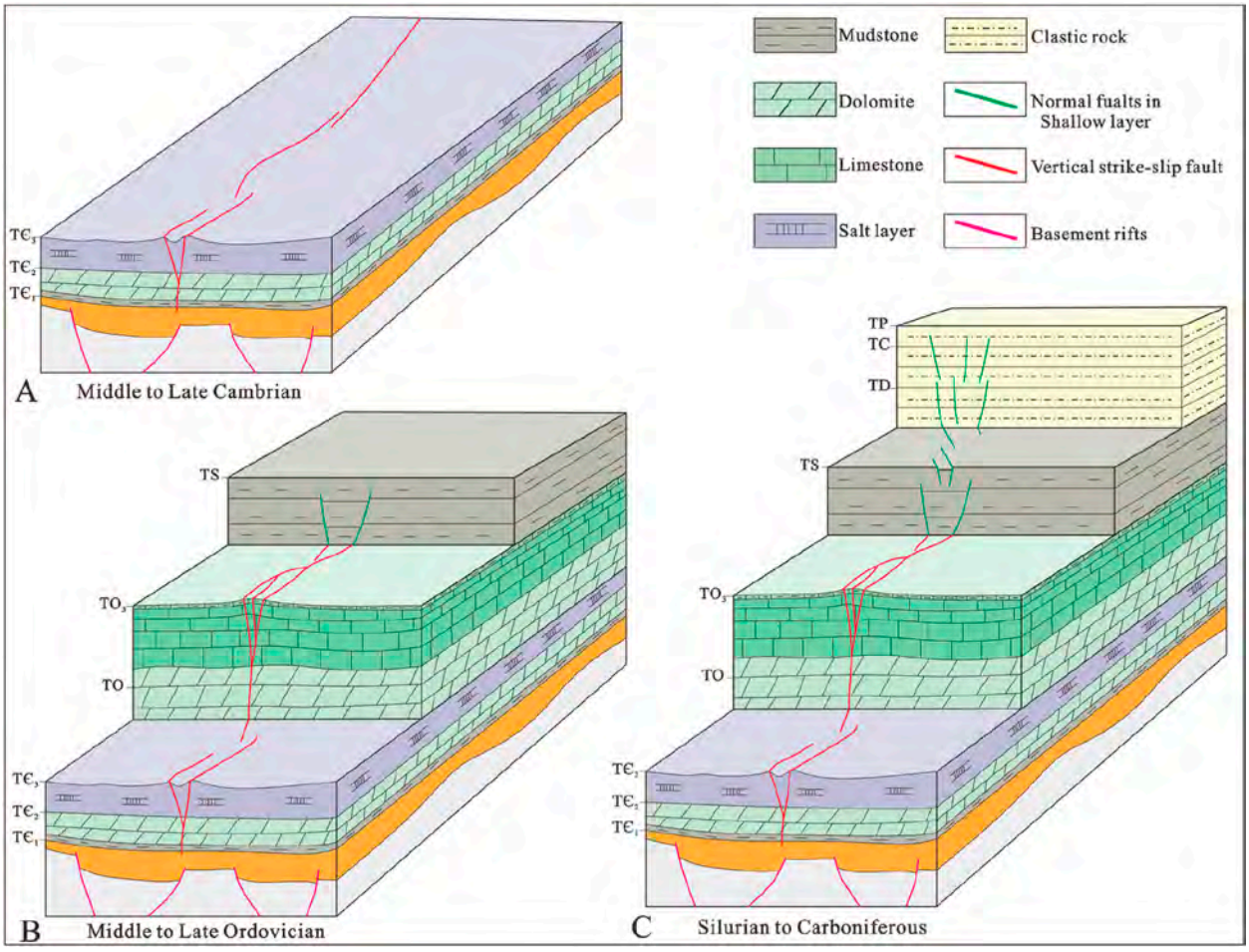

FIGURE 8
Active stages of the F_I17 fault: **(A)** Middle to Late Cambrian, **(B)** Middle to Late Ordovician; **(C)** Silurian to Carboniferous.

of normal faults in the profile may be related to the episodic activation of strike-slip faults, with a brief suspension in Devonian.

7 Discussion

7.1 Basement structure along the F_I17 fault

During the Nanhua-Sinian, the Tarim block separated from the Rodinia supercontinent, and the interior of the plate was under a strong extensional environment, while being influenced by the Rodinia superplume (Xu et al., 2009; Zhang et al., 2013). Cratonic intraplate continental rifts developed within the plate, and the rift system was widely distributed, leading to the heterogeneity of the pre-Cambrian basement structure within the plate (Zhu et al., 2017). Limited by the resolution of seismic data, the identification of the pre-Cambrian basement structure on the seismic profiles was restricted, but relying on the magnetic data within the basin, a preliminary understanding of the basement structural characteristics was obtained: the pattern of magnetic anomalies within the basin provides evidence of the Pre-Cambrian basement's spatial arrangement (Xu et al., 2005), which have a profound influence on the development of the NE trending strike-slip faults in the Tarim Uplift (Wu et al., 2011; Yang et al., 2013; Zhou et al., 2013; Lan et al., 2015). In recent years, with the advancement of geophysical technology, some scholars have carried out detailed studies on the pre-cambrian rift structure within some areas of the basin, depicting its development and distribution characteristics in profile and plan, showing that it has imposed significant impacts on the development of strike-slip faults above and hydrocarbon enrichment (Zhu et al., 2017; Wu et al., 2020b; Yi et al., 2020; Chen Y. Q. et al., 2022; Song et al., 2024b). In this research, we employed high-precision 3D seismic data from the Fuman Oilfield to meticulously delineate the structure of the pre-Cambrian basement and its planar distribution beneath the F_I17 fault (Figures 9, 10), and building upon prior investigations of various segments of the F_I17 fault (Liu and Deng, 2022; Li et al., 2023), to further dissect the basement characteristics of the F_I17 fault.

By identifying the bottom of the Sinian and the Cambrian on the seismic section, we can determine the thickness of the Sinian, which in turn reflects the characteristics of the pre-Cambrian basement structure. The map of Sinian thickness reveals that a series of basement rifts and uplifts have developed along the path of the F_I17 fault within the Manxi Low Uplift. These rifts exhibit a variety of

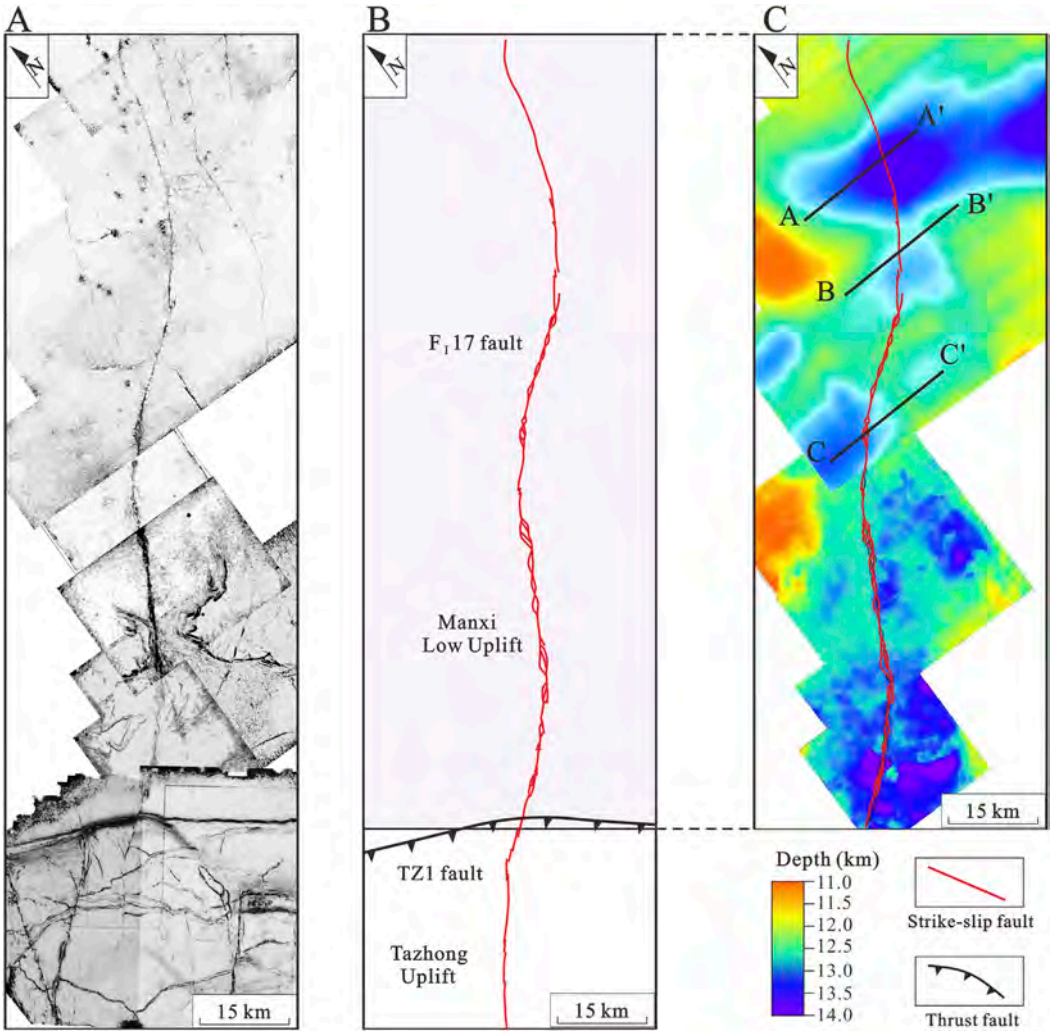

FIGURE 9
Uninterpreted **(A)** and interpreted **(B)** coherence slice of TO_3 interface (Modify from Liu and Deng, 2022; Li et al., 2023). **(C)** The thickness map of Precambrian strata.

sizes and orientations, with diameters spanning from 15 to 50 km (Figure 9C). The F_I17 fault cutting through the central or marginal of the rifts, interconnecting and extending, and exhibiting multiple deviations in their planar trend, presenting an overall S-shaped distribution. In profile, the basement structural characteristics are intricate, with widespread occurrence of rift structures, where the F_I17 fault is situated above a normal fault on the margin of the rift (Figures 10A, B), or located in the center of the rift (Figure 10C).

The development of faults generally exhibits inheritance, and pre-existing basement structures significantly impact the geometry and fault patterns (Chattopadhyay and Chakra, 2013). Basement heterogeneity influences the location, structural style, and evolution of subsequent faults. Faults are more prone to rupture along the edges or centers of rifts rather than in uplifts (Qi and Yang, 2010; Chen et al., 2023; Chen et al., 2024; Song et al., 2024b). Considering the trend deflection characteristics of the F_I17 fault within the Manxi Low Uplift and the distribution pattern of pre-Cambrian basement rifts, it can be inferred that the trend deflection of fault has been influenced by the distribution of pre-Cambrian rifts (pre-existing basement structures): the fault tends to initially rupture in small segments at the center and edges of the rifts and then expands and grows towards both ends. The interplay and linkage among these fragments, coupled with the non-linear planar arrangement of the rifts, culminate in the fault exhibiting a trajectory with several shifts (Figure 11).

7.2 Formation mechanism of F_I17 strike-slip fault

Previous researchers have conducted numerous studies on the formation mechanisms of strike-slip faults in the central Tarim basin, with a general consensus that the Tazhong and Tabei uplifts are characterized by simple shear (Neng et al., 2022; Chen et al., 2024) and X-type conjugate shear (Sun et al., 2021; Li, 2023; Song et al., 2024a), respectively. The major faults that cross structural

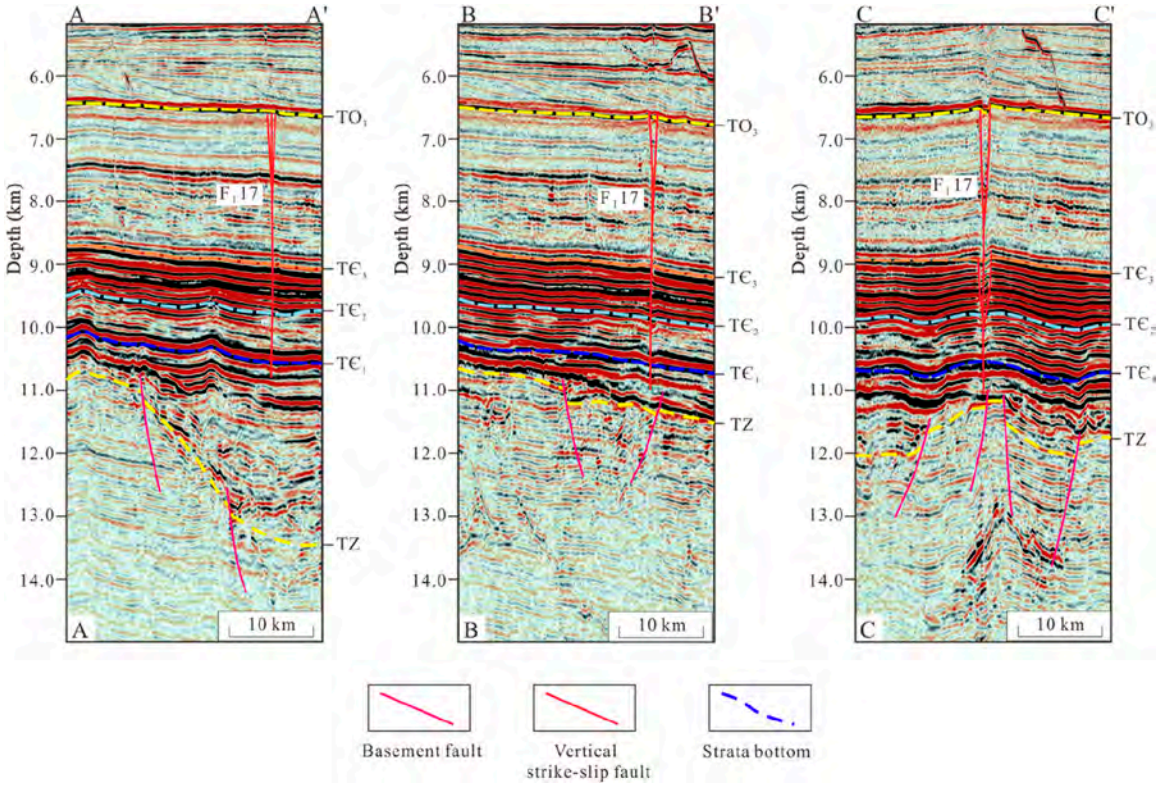

FIGURE 10
Typical seismic sections **(A–C)** of FI17 fault showing the basement structure. (for location, see Figure 9).

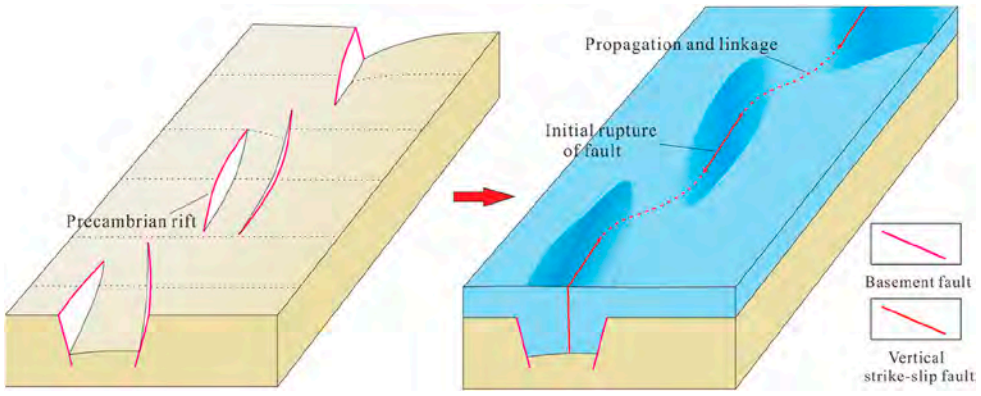

FIGURE 11
Propagation and linkage model of stike-slip faults under the control of precambrian rifts.

units and interconnect the two fault systems (such as the F_I5 and F_I17) play a significant role in displacement accommodation and transferring strain (Sun et al., 2021; Neng et al., 2022; Chen et al., 2024). Building on the understanding that basement rifts control the formation of overlying strike-slip faults (Figures 9–11), and integrating the tectonic evolution of the surrounding orogenic belts along with previous findings on the formation mechanism of the NEE-striking faults in Tazhong Uplift (Han et al., 2017; Chen et al., 2024), this paper establishes a formation and evolution mechanism for the F_I17 fault, which is governed by the heterogeneity of the basement.

During the Middle-Late Cambrian, influenced by the initial subduction of the Paleo-Asian Ocean to the north and the Proto-Tethys Ocean to the south (Mattern and Schneider, 2000; Xu et al., 2011; Han et al., 2015; Han et al., 2016), the central Tarim basin experienced weak compressional stress environment. Within the Manxi Low Uplift, basement rifts and uplifts are extensively distributed (Figures 9, 10), and under the influence of compressional

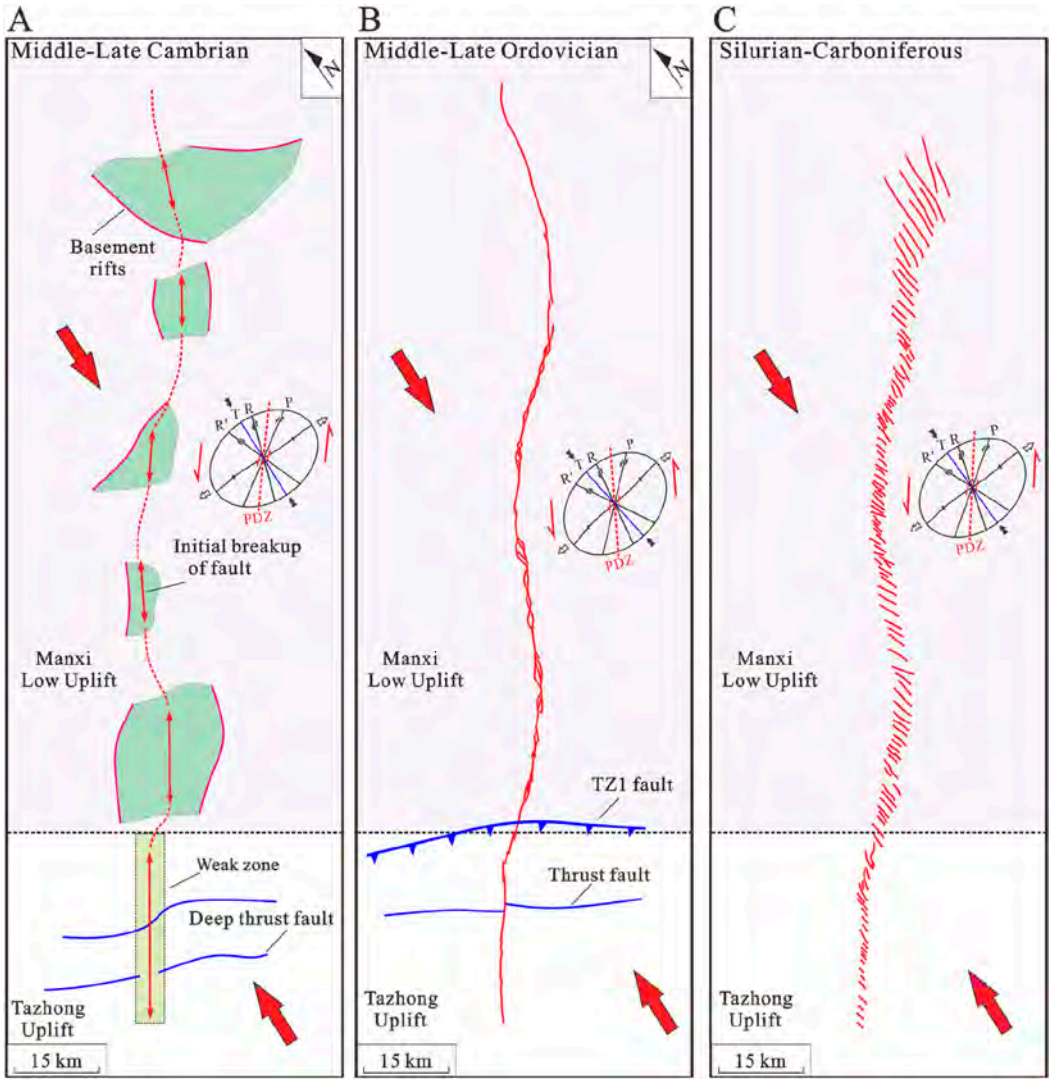

FIGURE 12
Formation mechanism and evolution processes of F_I17 fault. **(A)** Middle-Late Cambrian; **(B)** Middle-Late Ordovician; **(C)** Silurian-Carboniferous.

stress, rupture prior occurred at the edges and central parts of the rifts, forming a series of segments. Subsequently, during the growth and propagation process, the segments between different rifts interconnected, eventually forming a fault with multiple deviations in its planar trend. Within the Tazhong Uplift, strike-slip faults developed along the NE-trending weak zones under the influence of compressional stress (Han et al., 2017), primarily located at the bends and connective position of thrust faults (Chen et al., 2024), serving as tear faults that accommodate the displacement and strain of the thrust faults, which extend northward and connect with the strike-slip segments within the Mnaxi Low Uplift, forming the primary shape of the F_I17 fault (Figure 12A).

During the Middle-Late Ordovician, the closure of the Kunlun Ocean to the southwest (Li et al., 2009; Wu et al., 2012; Lan et al., 2015) and the initial subduction of the Altun Ocean to the southeast (Lan et al., 2015; Qiu et al., 2019) led to a strong compressive stress environment within the basin. The Tazhong and Tabei uplifts experienced a remarkable ascent (Li et al., 1996; Wang, 2004), and numerous intensely active thrust faults, such as the TZ1 fault, formed within the Tazhong Uplift (Lin et al., 2011; Lan et al., 2015). Under the strong compressional stress from the south, the F_I17 fault exhibited pronounced tectonic activity. However, within the Tazhong Uplift, the intensity of fault activity was considerably mitigated compared to that within the Manxi Low Uplift. This mitigation is attributed to the absorption and accommodation of the compressional strain by the thrust faults (Figure 12B).

During the Silurian-Carboniferous, the Altun Ocean underwent subduction and closure along the southeastern margin of the basin (Yang et al., 2005), and the South Tianshan Ocean to the north experienced a scissor-like closure from east to west (Chen et al., 1999; Gao and Fan, 2014), maintaining the basin under a compressional stress environment. The F_I17 fault underwent episodic reactivation, giving rise to groups of en-echelon normal faults (Figure 12C).

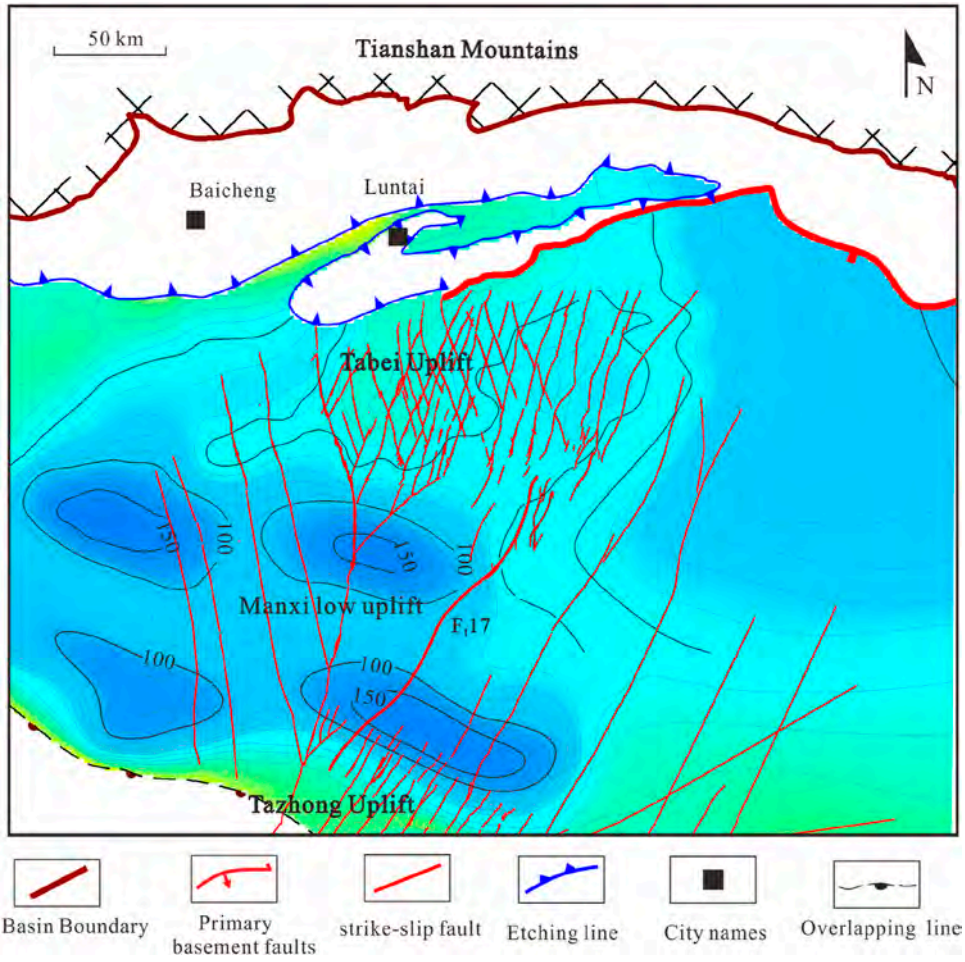

FIGURE 13
Map of Source Rock thickness distribution of the Yuertusi Formation in central Tarim basin.

7.3 Hydrocarbon enrichment factors of F_I17 fault

The F_I17 fault stands as one of the most productive strike-slip faults within the Tarim basin, boasting a series of prolific wells such as MS1, MS3, MS4, SB41, and SB42, each with a daily output over 1,000 tons of oil and gas equivalents (Liu and Deng, 2022; Liu et al., 2023). The fault zone is characterized by a scarcity of unsuccessful or inefficient wells; the majority of wells drilled have proven to be highly productive, with daily yields often exceeding a hundred tons. Moreover, within the Fuman Oilfield, the petroleum resource volume attributed to the F_I17 fault alone is estimated to exceed 2×10^8 tons (Tian et al., 2021). Previous studies on the ultra-deep strike-slip faults in the central Tarim Basin have revealed a fault-controlled, polycyclic hydrocarbon charging and accumulation system. The system is characterized by multi-stage Cambrian hydrocarbon supply and vertical hydrocarbon migration along the strike-slip faults, resulting in the formation of multi-layered composite hydrocarbon reservoirs (Qi, 2020; Wang et al., 2021). As one of the most petroliferous fault in the central Tarim basin, the factors influencing oil and gas enrichment of the F_I17 fault are likely associated with the distribution of source rocks, the development characteristics of the reservoirs, and the reactivation of the strike-slip fault.

Regarding the source rocks in the deep fault-controlled carbonate oil and gas reservoirs in the central Tarim basin, it is widely accepted that the Yuertusi Formation of the Lower Cambrian is the dominant source rock (Zhu et al., 2017; 2022; Tian et al., 2021). The Yuertusi Formation is a set of high-quality source rocks of the continental shelf slope-basin facies, characterized by a wide distribution, high organic matter abundance, and high maturity. The depositional center of the Yuertusi Formation is in the Manxi Low Uplift, where the maximum thickness can reach 200 m, and it thins out towards the Tabei and Tazhong uplifts. A robust hydrocarbon-generating center has developed within the Manxi Low Uplift, and the F_I17 fault is mainly located above the depositional center of the Yuertusi Formation in the Manxi Low Uplift (Figure 13), and the fault cuts through the Cambrian to communicate with the source rock (Figure 6), providing highly favorable conditions for hydrocarbon sources. The F_I17 fault's reservoir spaces consist of caverns and a network of fractures and voids, shaped by multiple episodes of strike-slip tectonic

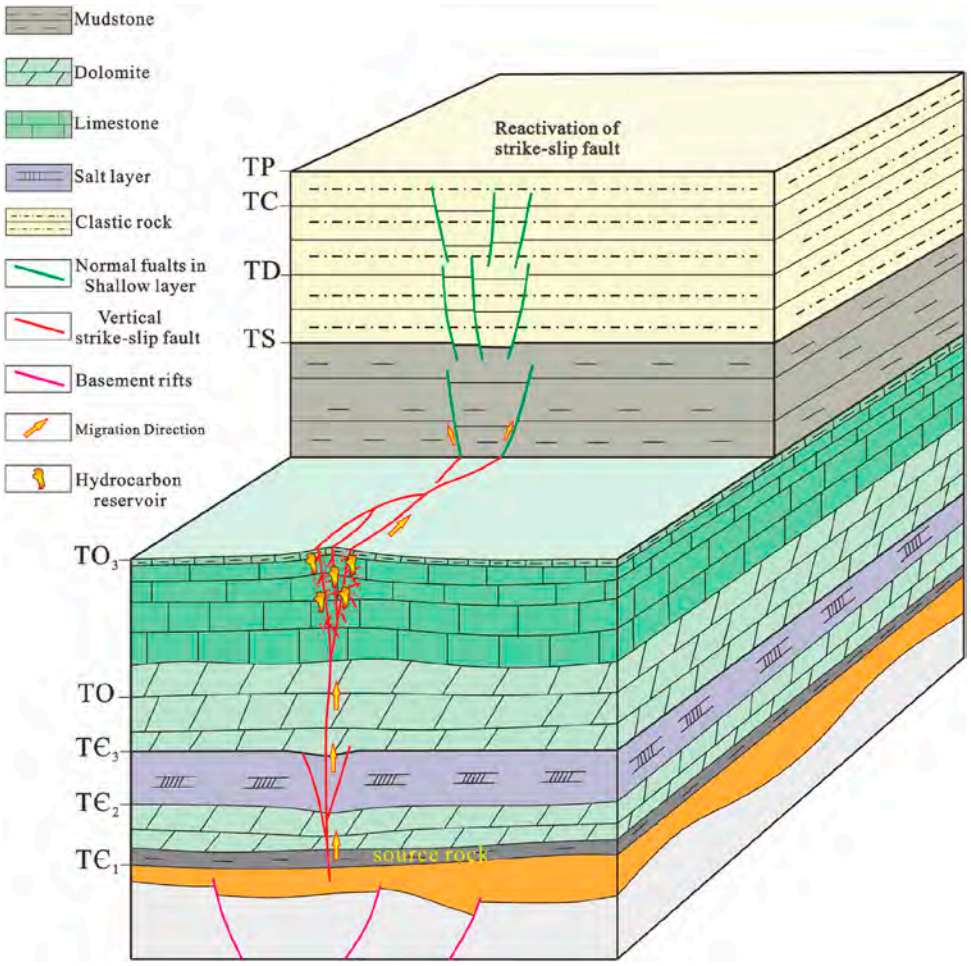

FIGURE 14
Hydrocarbon enrichment model of the F_I17 fault.

fracturing and material volume adjustments within the fault belt. The distribution of these reservoirs, constrained by the strike-slip fault, manifests as a ribbon-like pattern in plan view, with significant vertical development. Therefore, the pattern underpinned excellent conditions for reservoir development and the formation of large-scale reservoir bodies (Wang et al., 2022; Li et al., 2023). Recent studies suggest that the Yuertusi Formation's peak oil generation phase was during the Late Ordovician, with a transition to an advanced maturity gas generation phase in the Late Hercynian. The critical periods for hydrocarbon accumulation within the Manxi Low Uplift are identified as the Late Caledonian and Hercynian (Yang et al., 2022). The fault penetrated into the basement, linking the Yuertusi Formation with the Ordovician reservoir, serving as channel for deep fluid pulsating activity and hydrocarbon accumulation during its active phases. Therefore, the coupling relationship between the hydrocarbon generation phase of the source rock and the active period of faulting can control the degree of oil and gas enrichment (Wang Z. Y. et al., 2020; Song et al., 2023). The characteristics of normal fault development in the upper structural layer indicate that the F_I17 fault remained active during the Silurian-Carboniferous, aligning well with the hydrocarbon accumulation phase. This ensures that the fault, serving as a migration channel, remains permeable, thereby facilitating the vertical migration and effective charging of oil and gas (Figure 14).

8 Conclusion

1. The F_I17 fault exhibits characteristics of layered deformation structure, which can be divided into three structural layers. In the deep structural layer (below the $T\epsilon_3$ interface), basement rifts are developed with weak strike-slip deformation activity, and salt tectonic deformation is present within the Middle Cambrian. The middle structural layer ($T\epsilon_3$-TO_3 interface) is characterized by intense strike-slip deformation activity, with widespread development of flower-like structures. In the upper structural deformation layer (TO_3-TP) features the vertical development of three groups of en-echelon normal faults.
2. The formation of the F_I17 fault was controlled by the heterogeneity of the Precambrian basement structure, leading to multiple deflections in the fault plane's trend throughout its evolutionary process, which can be divided into three stages. During the Middle to Late Cambrian, under the influence of

weak compressive stress within the basin, rupture occurred along the basement rifts in the Manxi Low Uplift and the weak basement zones of the Tazhong Uplift, linking to form the fault's initial shape. In the Middle to Late Ordovician, under the action of strong compressive stress, the strike-slip fault intensely activated and propagated upwards. During the Silurian-Carboniferous, influenced by the progressive closure of surrounding oceans, the strike-slip fault experienced episodic reactivation, resulting in the formation of groups of normal faults in the upper structural layer.

3. The hydrocarbon enrichment of the F_I17 fault is jointly influenced by the distribution of hydrocarbon source rocks, the characteristics of reservoir development, and the reactivation of the strike-slip fault. The fault is situated above the depositional center of the source rocks, providing favorable conditions for oil sourcing; the intense fault activity has facilitated the development of large-scale fracture-cavity reservoirs; and the period of strike-slip fault reactivation coincides well with the hydrocarbon accumulation phase, favorable for the charging of hydrocarbon reservoirs.

Data availability statement

The original contributions presented in the study are included in the article/supplementary material, further inquiries can be directed to the corresponding author.

Author contributions

SC: Conceptualization, Formal Analysis, Writing–original draft, Writing–review and editing. XL: Investigation, Writing–review and editing. XS: Supervision, Writing–review and editing. YZ: Project administration, Writing–review and editing. ZX: Validation, Writing–review and editing. YN: Resources, Writing–review and editing. PK: Project administration, Writing–review and editing. JZ: Funding acquisition, Writing–review and editing.

Funding

The author(s) declare that financial support was received for the research, authorship, and/or publication of this article. This study was financially supported by the National Natural Sciences Foundation of China (Grant No. 42472186).

Conflict of interest

Authors YZ, ZX, and PK were employed by PetroChina Tarim Oilfield Company.

The remaining authors declare that the research was conducted in the absence of any commercial or financial relationships that could be construed as a potential conflict of interest.

Generative AI statement

The author(s) declare that no Generative AI was used in the creation of this manuscript.

Publisher's note

All claims expressed in this article are solely those of the authors and do not necessarily represent those of their affiliated organizations, or those of the publisher, the editors and the reviewers. Any product that may be evaluated in this article, or claim that may be made by its manufacturer, is not guaranteed or endorsed by the publisher.

References

Allen, M. B., Windley, B. F., and Zhang, C. (1993). Palaeozoic collisional tectonics and magmatism of the Chinese Tienshan, central Asia. *Tectonophysics* 220 (1-4), 89–115. doi:10.1016/0040-1951(93)90225-9

Chattopadhyay, A., and Chakra, M. (2013). Influence of pre-existing pervasive fabrics on fault patterns during orthogonal and oblique rifting: an experimental approach. *Mar. petroleum Geol.* 39 (1), 74–91. doi:10.1016/j.marpetgeo.2012.09.009

Chen, C. M., Lu, H. F., Jia, D., Cai, D. S., and Wu, S. M. (1999). Closing history of the southern Tianshan oceanic basin, western China: an oblique collisional orogeny. *Tectonophysics* 302 (1-2), 23–40. doi:10.1016/s0040-1951(98)00273-x

Chen, J. J., He, D. F., Tian, F. L., Huang, C., Ma, D. B., and Zhang, W. K. (2022a). Control of mechanical stratigraphy on the stratified style of strike-slip faults in the central Tarim Craton, NW China. *Tectonophysics* 830, 229307. doi:10.1016/j.tecto.2022.229307

Chen, S., Zhang, Y. T., Xie, Z., Song, X. G., and Liang, X. X. (2024). Multi-stages of paleozoic deformation of the fault system in the Tazhong uplift, Tarim Basin, NW China: implications for hydrocarbon accumulation. *J. Asian Earth Sci.* 265, 106086. doi:10.1016/j.jseaes.2024.106086

Chen, Y. J., Wu, Z. P., Su, W., Chen, M. M., Zhang, J., Liu, Y. Q., et al. (2023). Basement structures exert a crucial influence on the structural configuration of later rift development: insights from the Shanan and Chengbei sag, Bohai Bay Basin. *Mar. petroleum Geol.* 2023, 106272. doi:10.1016/j.marpetgeo.2023.106272

Chen, Y. Q., Wang, X. X., He, H., and Yi, Y. (2022b). Evolution of uplift and depression framework of Tarim craton in nanhua-cambrian. *China Pet. Explor.* 27 (4), 30–46. doi:10.3969/j.issn.1672-7703.2022.04.003

Deng, S., Li, H. L., Zhang, Z. P., Wu, X., and Zhang, J. B. (2018). Characteristics of differential activities in major strike-slip fault zones and their control on hydrocarbon enrichment in Shunbei area and its surroundings, Tarim Basin. *Oil Gas. Geol.* 39 (5), 878–888. doi:10.11743/ogg20180503

Deng, S., Li, H. L., Zhang, Z. P., Zhang, J. B., and Yang, X. (2019). Structural characterization of intracratonic strike-slip faults in the central Tarim Basin. *AAPG Am. Assoc. Pet. Geol. Bull.* 103 (1), 109–137. doi:10.1306/06071817354

Deng, S., Liu, Y. Q., Liu, J., Han, J., Wang, B., and Zhao, R. (2021). Structural styles and evolution models of intracratonic strike-slip faults and the implications for reservoir exploration and appraisal: a case study of the Shunbei area, Tarim Basin. *Geotect. Metallogenia* 45 (6), 1111–1126. doi:10.16539/j.ddgzyckx.2020.05.015

Deng, S., Zhao, R., Kong, Q., Li, Y., and Li, B. (2022). Two distinct Strike-Slip Fault networks in the Shunbei area and its surroundings, Tarim Basin: hydrocarbon accumulation, distribution, and controlling factors. *AAPG Bull.* 106 (1), 77–102. doi:10.1306/07202119113

Fan, C. H., Nie, S., Li, H., Radwan, A. E., Pan, Q. C., Shi, X. C., et al. (2024). Quantitative prediction and spatial analysis of structural fractures in deep shale gas reservoirs within complex structural zones: a case study of the Longmaxi Formation in the Luzhou area, southern Sichuan Basin, China. *J. Asian Earth Sci.* 263, 106025. doi:10.1016/j.jseaes.2024.106025

Gao, J., Long, L. L., Qian, Q., Huang, D. Z., Su, W., and Reiner, K. (2006). South tianshan: a late paleozoic or a triassic orogen? Acta petrol. *Sin.* 22 (5), 1049–1061. doi:10.3321/j.issn:1000-0569.2006.05.001

Gao, Z. Q., and Fan, T. L. (2014). Intra-platform tectono-sedimentary response to geodynamic transition along the margin of the Tarim Basin, NW China. *J. Asian Earth Sci.* 96, 178–193. doi:10.1016/j.jseaes.2014.08.023

Ge, R., Zhu, W., Wilde, S. A., He, J., Cui, X., Wang, X., et al. (2014). Neoproterozoic to Paleozoic long-lived accretionary orogeny in the northern Tarim Craton. *Tectonics* 33 (03), 302–329. doi:10.1002/2013tc003501

Han, B. F., He, G. Q., Wang, X. C., and Guo, Z. J. (2011). Late carboniferous collision between the Tarim and Kazakhstan-yili terranes in the western segment of the South tian Shan orogen, central asia, and implications for the northern Xinjiang, western China. *Earth Sci. Rev.* 109, 74–93. doi:10.1016/j.earscirev.2011.09.001

Han, X. Y., Deng, S., Tang, L. J., and Cao, Z. C. (2017). Geometry, kinematics and displacement characteristics of strike-slip faults in the northern slope of Tazhong uplift in Tarim Basin: a study based on 3D seismic data. *Mar. Petrol. Geol.* 88, 410–427. doi:10.1016/j.marpetgeo.2017.08.033

Han, Y., Zhao, G., Cawood, P. A., Sun, M., Eizenhofer, P. R., Hou, W., et al. (2016). Tarim and North China cratons linked to northern Gondwana through switching accretionary tectonics and collisional orogenesis. *Geology* 44 (02), 95–98. doi:10.1130/g37399.1

Han, Y., Zhao, G., Sun, M., Eizenhofer, P. R., Hou, W., Zhang, X., et al. (2015). Paleozoic accretionary orogenesis in the Paleo-Asian Ocean: insights from detrital zircons from silurian to carboniferous strata at the northwestern margin of the Tarim craton. *Tectonics* 34 (02), 334–351. doi:10.1002/2014tc003668

He, D. F., Jia, C. Z., Li, D. S., Zhang, C. J., Meng, Q. R., and Shi, X. (2005). Formation and evolution of polycyclic superimposed Tarim Basin. Oil. *Gas. Geol.* 26 (01), 64–77. doi:10.11743/ogg20050109

Jia, C. Z. (1997). *Tectonic characteristics and petroleum, Tarim Basin. China. Pet.* Beijing: Ind. Press, 1–120.

Jia, C. Z., and Wei, G. Q. (2002). Structural characteristics and petroliferous features of Tarim Basin. *Chin. Sci. Bull.* 47, 1–11. doi:10.1007/bf02902812

Jiao, F. Z. (2017). Significance of oil and gas exploration in NE strike-slip fault belts in Shuntuoguole area of Tarim Basin. *Oil Gas. Geol.* 38 (5), 831–839. doi:10.11743/ogg20170501

Lan, X. D., Lü, X. X., Zhu, Y. M., and Yu, H. F. (2015). The geometry and origin of strike-slip faults cutting the Tazhong low rise megaanticline (central uplift, Tarim Basin, China) and their control on hydrocarbon distribution in carbonate reservoirs. *J. Nat. Gas. Sci. Eng.* 22, 633–645. doi:10.1016/j.jngse.2014.12.030

Li, D. S., Liang, D. G., Jia, C. Z., Wang, G., Wu, Q. Z., and He, D. F. (1996). Hydrocarbon accumulation in the Tarim Basin, China. *AAPG Bulletin* 80 (10), 1587–1603.

Li, C. X., Jia, C. Z., Li, B., Yang, G., Yang, H. J., Luo, C. S., et al. (2009). Distribution and tectonic evolution of the Paleozoic fault system, the north slope of Tazhong uplift, Tarim Basin. *Acta Geol. Sin.* 83 (8), 1065–1073. doi:10.3321/j.issn:0001-5717.2009.08.002

Li, C. X., Wang, X. F., Li, B. L., and He, D. F. (2013). Paleozoic fault systems of the Tazhong uplift, Tarim Basin, China. *Pet. Geol.* 39 (1), 48–58. doi:10.1016/j.marpetgeo.2012.09.010

Li, H. (2023). Deciphering the formation period and geological implications of shale tectonic fractures: a mini review and forward-looking perspectives. *Front. Energy Res.* 11, 1320366. doi:10.3389/fenrg.2023.1320366

Li, H., Tang, H. M., Qin, Q. R., Zhou, J. L., Qin, Z. J., Fan, C. H., et al. (2019). Characteristics, formation periods and genetic mechanisms of tectonic fractures in the tight gas sandstones reservoir: a case study of Xujiahe Formation in YB area, Sichuan Basin, China. *J. Petroleum Sci. Eng.* 178, 723–735. doi:10.1016/j.petrol.2019.04.007

Li, H. Y., Han, J., Chen, P., Li, Y., and Bu, X. Q. (2023). Deformation and favorable area evaluation of Shunbei No.4 strike-slip fault zone in Tarim Basin. *Xinjiang Pet. Geol.* 44 (2), 127–135. doi:10.7657/XJPG20230201

Li, S. T., Ren, J. Y., Xing, F. C., Liu, Z. H., Li, H. Y., Chen, Q. L., et al. (2012). Dynamic processes of the Paleozoic Tarim basin and its significance for hydrocarbon accumulation-a review and discussion. *J. Earth Sci.* 23, 381–394. doi:10.1007/s12583-012-0262-5

Li, Z. L., Chen, H. L., Song, B., Li, Y. Q., Yang, S. F., and Yu, X. (2011). Temporal evolution of the Permian large igneous province in Tarim Basin in northwestern China. *J. Asian Earth Sci.* 42, 917–927. doi:10.1016/j.jseaes.2011.05.009

Lin, C. S., Li, S. T., Liu, J. Y., Qian, Y. X., Luo, H., Chen, J. Q., et al. (2011). Tectonic framework and paleogeographic evolution of the Tarim basin during the Paleozoic major evolutionary stages. *Acta Petrol. Sin.* 27 (1), 210–218.

Liu, Q., Zhang, Y. T., Chen, S., Song, X. G., Li, T., Kang, P. F., et al. 2023. Analysis of development and evolution characteristics of strike-slip faults in Tarim Basin and its geological significance: a case study of $F_1$17 fault in fuman oilfield. 37 (5), 1123–1135 .

Liu, Y. J., Neubauer, F., Genser, J., Ge, X. H., Takasu, A., Yuan, S. H., et al. (2007). Geochronology of the initiation and displacement of the Altyn strike-slip fault, western China. *J. Asian Earth Sci.* 29 (2-3), 243–252. doi:10.1016/j.jseaes.2006.03.002

Liu, Y. Q., and Deng, S. (2022). Structural analysis of intraplate strike-slip faults with small to medium displacement: a case study of the Shunbei 4 fault,Tarim Basin. *J. China Univ. Min. and Technol.* 51 (1), 124–136. doi:10.13247/j.cnki.jcumt.001324

Mattern, F., and Schneider, W. (2000). Suturing of the Proto- and paleo-tethys oceans in the western Kunlun (Xinjiang, China). *J. Asian Earth Sci.* 18, 637–650. doi:10.1016/s1367-9120(00)00011-0

Neng, Y., Li, Y., Qi, J. F., Ma, X., Zuo, L., and Chen, P. (2022). Deformation styles and multi-stage evolution history of a large intraplate Strike-Slip Fault system in a paleozoic superimposed basin: a case study from the Tarim Basin, NW China. *Front. Earth Sci.* 10, 837354. doi:10.3389/feart.2022.837354

Qi, J. F., and Yang, Q. (2010). Cenozoic structural deformation and dynamic processes of the Bohai Bay basin province, China. *Mar. Petroleum Geol.* 27 (4), 757–771. doi:10.1016/j.marpetgeo.2009.08.012

Qi, L. X. (2020). Characteristics and inspiration of ultra-deep fault-karst reservoir in the Shunbei area of the Tarim Basin. *China Pet. Explor.* 25 (1), 102–111. doi:10.3969/j.issn.1672-7703.2020.01.010

Qiu, H. B., Deng, S., Cao, Z. C., Yin, T., and Zhang, Z. P. (2019). The evolution of the complex anticlinal belt with crosscutting strike-slip faults in the central Tarim basin, NW China. *Tectonics* 38, 2087–2113. doi:10.1029/2018tc005229

Ren, J. Y., Zhang, J. X., Yang, H. Z., Hu, D. S., Li, P., and Zhang, Y. P. (2011). Analysis of fault systems in the central uplift, Tarim basin. *Acta Petrol. Sin.* 27, 219–230.

Sharps, R., McWilliams, M., Li, Y. P., Cox, A., Zhang, Z. K., Zhai, Y. J., et al. (1989). Lower Permian paleomagnetism of the Tarim block, northwestern China. *Earth Planet Sci. Lett.* 92, 275–291. doi:10.1016/0012-821x(89)90052-6

Shen, Z. Y., Neng, Y., Han, J., Huang, C., Zhu, X. X., Chen, P., et al. (2022). Structural styles and linkage evolution in the middle segment of a strike-slip fault: a case from the Tarim Basin, NW China. *J. Struct. Geol.* 157, 104558. doi:10.1016/j.jsg.2022.104558

Song, X. G., Chen, S., Xie, Z., Kang, P. F., Li, T., Yang, M. H., et al. (2023). Strike-slip faults and hydrocarbon accumulation in the eastern part of Fuman oilfield, Tarim Basin. *Oil and Gas Geol.* 44 (2), 335–349. doi:10.11743/ogg20230207

Song, X. G., Chen, S., Zhang, Y. T., Xie, Z., Liang, X. X., Yang, M. H., et al. (2024a). Formation mechanism of the small-angle X-type strike-slip faults in deep basin and its controlling on hydrocarbon accumulation: a case study from the Tabei Uplift, Tarim Basin, NW China. *Front. earth Sci.* 12, 1387544. doi:10.3389/feart.2024.1387544

Song, X. G., Chen, S., Zhang, Y. T., Xie, Z., Neng, Y., Liang, X. X., et al. (2024b). New insights into the evolution and formation mechanism of SB5 fault: a case study from the Fuman Oilfield, Tarim basin, NW China. *Front. earth Sci.* 12, 1416850. doi:10.3389/feart.2024.1416850

Sun, Q. Q., Fan, T. L., Gao, Z. Q., Wu, J., Zhang, H. H., Qi, J., et al. (2021). New insights on the geometry and kinematics of the Shunbei 5 strike-slip fault in the central Tarim Basin, China. *J. Struct. Geol.* 150, 104400. doi:10.1016/j.jsg.2021.104400

Tang, L. J. (1994). Evolution and tectonic patterns of Tarim Basin. *Earth Sci.* 19 (06), 742–754. doi:10.3321/j.issn:1000-2383.1994.06.006

Teng, C. Y., Cai, Z. X., Hao, F., and Cao, Z. C. (2020). Structural geometry and evolution of an intracratonic strike-slip fault zone: a case study from the north SB5 fault zone in the Tarim Basin, China. *Jorunal Struc Geo* 140, 104159. doi:10.1016/j.jsg.2020.104159

Tian, J., Yang, H. J., Zhu, Y. F., Deng, X. L., Xie, Z., Zhang, Y. T., et al. (2021). Geological conditions for hydrocarbon accumulation and key technologies for exploration and development in Fuman oil field, Tarim Basin. *Acta Pet. Sin.* 42 (8), 971–985. doi:10.7623/syxb202108001

Wang, B., Zhao, Y. Q., He, S., Guo, X. W., Cao, Z. C., Deng, S., et al. (2020a). Hydrocarbon accumulation stages and their controlling factors in the northern Ordovician Shunbei 5 fault zone,Tarim Basin. *Oil and Gas Geol.* 41 (5), 965–974. doi:10.11743/ogg20200507

Wang, Q. H. (2023). Differential deformation and evolution characteristics of the no. 17 strike-slip fault zone in the Tarim basin. *Geoscience* 37 (05), 1136–1145. doi:10.19657/j.geoscience.1000-8527.2022.090

Wang, Q. H., Yang, H. J., Li, Y., Lü, X. X., Zhang, Y. T., Zhang, Y. Q., et al. (2022). Control of strike-slip fault on the large carbonate reservoir in Fuman, Tarim Basin-a reservoir mode. *Earth Sci. Front.* 29 (6), 239–251. doi:10.13745/j.esf.sf.2022.8.17

Wang, Q. H., Yang, H. J., Wang, R. J., Li, S. Y., Deng, X. L., Li, Y., et al. (2021). Discovery and exploration technology of fault-controlled large oil and gas fields of ultra-deep formation in strike slip fault zone in Tarim Basin. *China Pet. Explor.* 26 (4), 58–71. doi:10.3969/j.issn.1672-7703.2021.04.005

Wang, Y. Y., Chen, J. F., Pang, X. Q., Wang, G., Hu, T., Zhang, B. S., et al. (2017). Hydrocarbon migration along fault intersection zone—a case study on Ordovician carbonate reservoirs in Tazhong area, Tarim Basin, NW China. *Geol. J.* 52 (5), 832–850. doi:10.1002/gj.2850

Wang, Z. H. (2004). Tectonic evolution of the western Kunlun orogenic belt, western China. *J. Asian Earth Sci.* 24 (2), 153–161. doi:10.1016/j.jseaes.2003.10.007

Wang, Z. Y., Gao, Z. Q., Fan, T. L., Shang, Y. X., Qi, L. X., and Yun, L. (2020b). Structural characterization and hydrocarbon prediction for the SB5M strikeslip fault zone in the Shuntuo Low Uplift, Tarim Basin. *Mar. Petroleum Geol.* 117, 104418. doi:10.1016/j.marpetgeo.2020.104418

Windley, B. F., Allen, M. B., Zhang, C., Zhao, Z. Y., and Wang, G. R. (1990). Paleozoic accretion and cenozoic redeformation of the Chinese tien Shan range, central asia. *Geology* 18 (2), 128–131. doi:10.1130/0091-7613(1990)018<0128:paacro>2.3.co;2

Wu, G. H., Cheng, L. F., Liu, Y. K., Wang, H., Qu, T. L., and Gao, L. (2011). Strike-slip fault system of the cambrian-Ordovician and its oil-controlling effect in Tarim Basin. Xinjiang Pet. *Geol.* 32 (3), 239–243.

Wu, G. H., Deng, W., Huang, S. Y., Zheng, D. M., and Pan, W. Q. (2020b). Tectonic-paleogeographic evolution in the Tarim Basin. *Chin. J. Geol.* 52 (2), 305–321. doi:10.12017/dzkx.2020.020

Wu, G. H., Kim, Y.-S., Su, Z., Yang, P. F., Ma, D. B., and Zheng, D. M. (2020a). Segment interaction and linkage evolution in a conjugate strike-slip fault system from the Tarim Basin, NW China. *Mar. Petrol. Geol.* 112, 104054. doi:10.1016/j.marpetgeo.2019.104054

Wu, G. H., Xiao, Y., He, J. Y., Chen, Z. Y., He, S., and Zhu, G. Y. (2019). Geochronology and geochemistry of the late Neoproterozoic A-type granitic clasts in the southwestern Tarim Craton: petrogenesis and tectonic implications. *Int. Geol. Rev.* 61 (03), 280–295. doi:10.1080/00206814.2017.1423521

Wu, G. H., Yang, H. J., Qu, T. L., Li, H. W., Luo, C. S., and Li, B. L. (2012). The fault system characteristics and its controlling roles on marine carbonate hydrocarbon in the Central uplift, Tarim basin. Acta Petrol. *Sin.* 28 (3), 793–805.

Wu, L., Guan, S. W., Zhang, S. C., Yang, H. J., Jin, J. Q., Zhang, X. D., et al. (2018). Neoproterozoic stratigraphic framework of the Tarim craton in NW China: implications for rift evolution. *J. Asian Earth Sci.* 158, 240–252. doi:10.1016/j.jseaes.2018.03.003

Xu, B., Xiao, S. H., Zou, H. B., Chen, Y., Li, Z. X., Song, B., et al. (2009). SHRIMP zircon U-Pb age constraints on Neoproterozoic Quruqtagh diamictites in NW China. *Precambrian Res.* 168 (3-4), 247–258. doi:10.1016/j.precamres.2008.10.008

Xu, M. J., Wang, L. S., Zhong, K., Hu, D. Z., Li, H., and Hu, X. Z. (2005). Features of gravitational and magnetic fields in the Tarim Basin and basement structure analysis. *Geol. J. China Univ.* 11 (4), 585–592. doi:10.3969/j.issn.1006-7493.2005.04.015

Xu, X., Zuza, A. V., Yin, A., Lin, X. B., Chen, H. L., and Yang, S. F. (2021). Permian PlumeStrengthened Tarim Lithosphere controls the Cenozoic deformation pattern of the Himalayan-Tibetan orogen. *Geology* 49 (1), 96–100. doi:10.1130/g47961.1

Xu, Z. Q., Li, S. T., Zhang, J. X., Yang, J. S., He, B. Z., Li, H. B., et al. (2011). Paleo-Asian and Tethyan tectonic systems with docking the Tarim block. *Acta Petro Sin.* 27 (01), 1–22.

Yang, S., Wu, G. H., Zhu, Y. F., Zhang, Y. T., Zhao, X. X., Lu, Z. Y., et al. (2022). Key oil accumulation periods of ultra-deep fault-controlled oil reservoir in northern Tarim Basin, NW China. *Petroleum Explor. Dev.* 49 (2), 285–299. doi:10.1016/s1876-3804(22)60024-7

Yang, S. B., Liu, J., Li, H. L., Zhang, Z. P., and Li, Q. Q. (2013). Characteristics of the NE-trending strike-slip fault system and its control on oil accumulation in north peri-cline area of the Tazhong paleouplift. *Oil Gas. Geol.* 34 (6), 797e802. doi:10.11743/ogg20130612

Yang, S. F., Chen, H. L., Ji, D. W., Li, Z. L., Dong, C. W., Jia, C. Z., et al. (2005). Geological process of early to middle Permian Magmatism in Tarim Basin and its geodynamic significance. *Geol. J. China Univ.* 11 (4), 504–511. doi:10.3969/j.issn.1006-7493.2005.04.005

Yao, Y. T., Zeng, L. B., Mao, Z., Han, J., Cao, D. S., and Lin, B. (2023). Differential deformation of a strike-slip fault in the Paleozoic carbonate reservoirs of the Tarim Basin, China. *J. Struc Geo* 173, 104908. doi:10.1016/j.jsg.2023.104908

Yi, S. W., Li, M. P., Guo, X. J., Fan, T. Z., Yang, F., Fang, H., et al. (2020). Control of the Nanhua paleo-rift on cambrian sedimentation and its exploration significance in Tarim Basin. *Acta Pet. Sin.* 41 (11), 1293–1308. doi:10.7623/syxb202011001

Yu, Y. X., Tang, L. J., Yang, W. J., Huang, T. Z., Qiu, N. S., and Li, W. G. (2014). Salt structures and hydrocarbon accumulations in the Tarim Basin, northwest China. *AAPG Bull.* 98, 135–159. doi:10.1306/05301311156

Zhang, C. L., Li, Z. X., Li, X. H., and Ye, H. M. (2009). Neoproterozoic mafic dyke swarms at the northern margin of the Tarim Block, NW China: age, geochemistry, petrogenesis and tectonic implications. *J. Asian Earth Sci.* 35, 167–179. doi:10.1016/j.jseaes.2009.02.003

Zhang, C. L., Zhou, H. B., Li, H. K., and Wang, H. Y. (2013). Tectonic framework and evolution of the Tarim block in NW China. *Gondwana Res.* 23 (4), 1306–1315. doi:10.1016/j.gr.2012.05.009

Zhang, G. Y., Zhao, W. Z., Wang, H. J., Li, H. H., and Liu, L. (2007). Multicycle tectonic evolution and composite petroleum systems in the Tarim Basin. *Oil Gas. Geol.* 28, 653–663. doi:10.3321/j.issn:0253-9985.2007.05.017

Zhang, Z. S., Li, M. J., and Liu, S. P. (2002). Generation and evolution of Tazhong low uplift. *Petrol. explor. Dev.* 29 (1), 28–31. doi:10.3321/j.issn:1000-0747.2002.01.007

Zheng, M. L., Wang, Y., Jin, Z. J., Li, J. C., Zhang, Z. P., Jiang, H. S., et al. (2014). Superimposition, evolution and petroleum accumulation of Tarim Basin. *Oil Gas. Geol.* 35 (6), 925–934. doi:10.11743/ogg20140619

Zhou, X. Y., Lv, X. X., Yang, H. J., Wang, Y., Yu, H. F., Cai, J., et al. (2013). Effects of strike-slip faults on the differential enrichment of hydrocarbons in the northern slope of Tazhong area. *Acta Pet. Sin.* 34 (4), 628–637. doi:10.7623/syxb201304002

Zhu, G. Y., Hu, J. F., Chen, Y. Q., Xue, N., Zhao, K., Zhang, Z. Y., et al. (2022). Geochemical characteristics and formation environment of source rock of the Lower Cambrian Yuertusi Formation in well Luntan 1in Tarim basin. *Acta Geol. Sin.* 96 (6), 2116–2130. doi:10.19762/j.cnki.dizhixuebao.2022285

Zhu, G. Y., Ren, R., Chen, F. R., Li, T. T., and Chen, Y. Q. (2017). Neoproterozoic Rift basins and their control on the development of hydrocarbon source rocks in the Tarim Basin, NW China. *J. Asian Earth Sci.* 150, 63–72. doi:10.1016/j.jseaes.2017.09.018